ARISTOTLE UNIVERSITY OF THESSALONIKI
FACULTY OF ENGINEERING
DEPARTMENT OF ELETRICAL AND COMPUTER ENGINEERING

Diploma Thesis

Inverse problem solving in microwave tomography applications using the finite element method (FEM) contrast source inversion (CSI)

Ioannis Vogiatzis Oikonomidis

Supervisor: Traianos Yioultis, Assistant professor

THESSALONIKI JULY 2012

Inverse problem solving in microwave tomography applications using the finite element method (FEM) contrast source inversion (CSI)

CONTENTS

1. INTRODUCTION

1.1 Preface

The subject of my thesis leading to my five year diploma acquisition, that has been the main occupation during my final year in the department of Electrical and Computer Engineering of Aristotle University of Thessaloniki concerns microwave tomography. A novel imaging technique is studied and implemented that uses microwaves and inverse scattering methods for the quantitative reconstruction of the dielectric properties of the materials inside an imaging domain. Inverse scattering problems are characterized as ill-posed problems and require special treatment during solving.

As a biomedical technique, microwave tomography is a promising alternative to current methods. It uses non ionizing radiation, it is a low-cost technique, especially in comparison with magnetic resonance imaging (MRI) and it has the ability to image bulk electrical properties as a feature of tissue that is not imaged by most other schemes. Additionally, it can quantitatively reconstruct frequency dependent permittivity and conductivity profiles of living tissues as a way of identifying physiological conditions of those tissues

The object of interest is illuminated by a number of electromagnetic radiation sources located on a measurement surface. By measuring the scattered field, an optimization problem is being solved, over variables that are connected with the dielectric properties of the object that are to be reconstructed. This reconstruction problem is highly nonlinear thus requiring regularization for solving, since a direct estimate tends to lead to poor results. The most common way for solving such kind of problems is the constant minimization of a cost functional through conjugated gradient techniques.

1.2 Outline of the thesis

In the second chapter of the current thesis a technique for calculating the electromagnetic scattering from a 2D arbitrarily shaped scatterer illuminated by a TM wave is presented. The mathematical formulation that characterizes the problem and the finite element method (FEM) are also outlined. The FEM method the domain is discretized in simple geometrical shapes for the solution of the Maxwell and Helmholtz equations that characterize our problem. Since open regions are studied, the infinite

region must be truncated with suitable boundary conditions in order to limit the size of the computational domain. In the current thesis the perfectly matched layers were selected and a short presentation of them is given in chapter 2.

In the third chapter a definition of the inverse problem is given and some methods for solving it are presented. The iterative Contrast Source Inversion (CSI) method is outlined with detail, as well as its variations the FEM-CSI and FEM-MRCSI methods, both using finite elements on the contrary with the original method that is based on integral equations formulations and Green functions.

Using the methods described in the previous chapters, chapter four focuses on their development in MATLAB using in house programming as no commercial packages were used. The implemented algorithms are evaluated on synthetic datasets due to the absence of an experimental scheme. Using the methods of chapter 2 in the resulting scattered fields noise addition was implemented in order to ensure better evaluation. Consequently the reconstruction results for a number of different scatterers are given. Finally a proposal for a different definition of the problem variables is made and the problems outlined in its evaluation are given.

In the fifth and final chapter, the thesis is concluded along with some future research proposals.

In this part I would like to acknowledge my supervisor professor Trainos Yioultsis for his constant scientific guidance, his support and his unflagging interest throughout my thesis work.

2. SOLVING SCATTERING PROBLEMS

2.1 The finite element method (FEM)

Electromagnetic scattering problems are mostly differential equations problems, which in many cases do not have an analytical solution. A computational method for solving such problems is the finite element method (FEM) [1]. It constitutes a general method for solving differential equations over a domain Ω, which is discretized in simple geometric shapes (figure 2.1.1). To begin with the problem's degrees of freedom are selected, namely the unknowns of the problem, which in the simplest formulations are the values of the unknown variable in the nodes of the generated mesh. Consequently, according to the degrees of freedom that have been selected an approximate formula for the unknowns of the problem, usually of low polynomial order inside the element. Subsequently, the problem is reformulated using a variational, either with help of a functional, the minimization of which leads to a characteristic differential equation, or using weighted residuals on the differential equation. Finally, after the reformulation of the problem with one of the previously mentioned techniques a linear system of equations is formed in respect to the problems selected degrees of freedom.

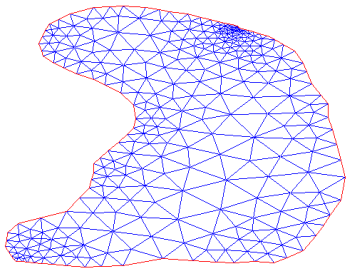

Figure 2.1.1. Domain discretization in finite elements

2.2 Triangular finite elements – Simplex coordinates

In two dimensions electromagnetic problems where the unknown variable is scalar, triangular elements are frequently used, with the unknown quantity residing in the vertices of the triangles (first order triangular element). The triangular element is the simplest form or shape simplex in two dimensions (figure 2.2.1).

In spite of the fact that other elements can also be used (quadrilateral -2D, tetrahedral hexahedral -3D) simplex elements are the simplest ones having also the advantage of better discretization of arbitrarily shaped geometries.

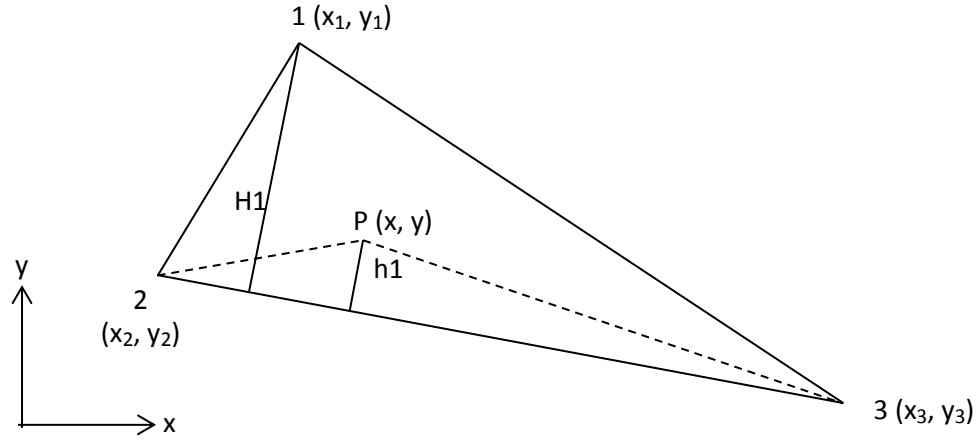

Figure 2.2.1. Triangular finite element and simplex coordinate definition

If coordinates relative to the nodes of the element are chosen for the analysis of our problem and not the standard Cartesian coordinate system, the problem's complexity is significantly minimized. The *simplex coordinates* ζ_1, ζ_2, ζ_3 of a point (x,y) can be defined as $\zeta_1 = h_1/H_1$, where h_1 is the distance of the point from the side [2,3] and H_1 is the height from the vertex 1. Coordinates ζ_2, ζ_3 can be defined in a similar way. An equivalent formulation is $\zeta_1 = (P12)/(123)$, where $(P12)$ (123) are the areas of the triangles $(P12)$ and (123) accordingly [1]. By using detriments to calculate the areas in the previous definition, the following formula (2.1) for the simplex coordinates can be easily derived.

$$\zeta_1 = \frac{x_2 y_3 - x_3 y_2}{D} + \frac{y_2 - y_3}{D} x + \frac{x_3 - y_2}{D} y \tag{2.1}$$

D is the unsigned detriment whose absolute value is equal with double the area of the element. Define

$$a_1 = \frac{x_2 y_3 - x_3 y_2}{D},\ b_1 = \frac{y_2 - y_3}{D},\ c_1 = \frac{x_3 - y_2}{D} \tag{2.2}$$

Then $\zeta_1 = a_1 + b_1 x + c_1 y$ is a linear equation that combines the simplex with the Cartesian coordinates. In general $\zeta_i = a_i + b_i x + c_i y$, $i=1,2,3$ with the coefficients a_i, b_i, c_i easily calculated by circular changing indices. Simplex ζ_i has the property:

$$\zeta_i = \begin{cases} 1 & \text{in node i} \\ 0 & \text{in other nodes} \end{cases} \tag{2.3}$$

The variation of ζ_i inside the element is linear, with its contours being parallel to the side where node i does not belong to (figure 2.2.2). Finally by the definition of the simplex coordinates and the equality $(P12)+(P23)+(P13)=(123)$ it can be easily shown that

$$\zeta_1+\zeta_2+\zeta_3=1 \tag{2.4}$$

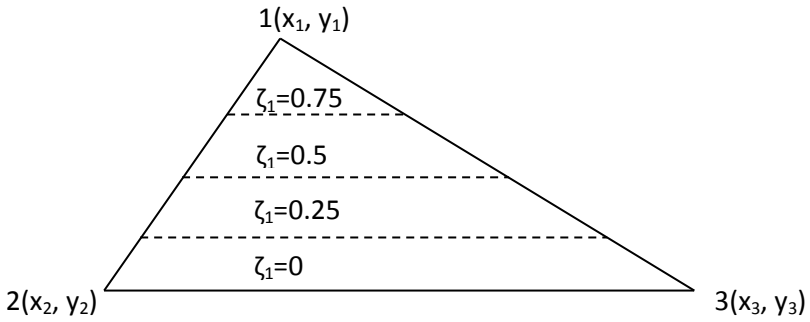

Figure 2.2.2. Contour plots of simplex coordinate for node 1

The next step is to determine the approximation of the unknown variable. Let φ an unknown scalar function. If the values of φ at the nodes of the element $(\varphi_1, \varphi_2, \varphi_3)$ are considered as degrees of freedom, then inside the element $\varphi = \varphi_1 N_1+\varphi_2 N_2+\varphi_3 N_3$, where N_i $i=1,2,3$ the base functions that are yet to be determined. Since $\varphi|_{(1)}=\varphi_1$ it can be easily assumed that $N_1|_{(1)}=1$, where $N_1|_{(2)}= N_1|_{(3)}=0$. Hence it would be logical to define

$$N_i=\zeta_i \ , \ i=1,2,3 \tag{2.5}$$

The unknown function is given by the equation (2.6) and it is partially a linear approximation inside each separate element. It must be noted that equation (2.6) is valid only for a single specific element. By taking into account all the elements that node i belong, the base function would have the form of a pyramid (figure 2.2.3). It is clear that all the partial contributions from the different individual elements must be added. This technique is known as assembly [1].

$$\varphi=\sum_{i=1}^{3}\varphi_i N_i \tag{2.6}$$

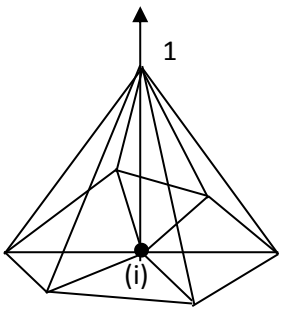

Figure 2.2.3. Total base function of node (i)

2.3 Galerkin formulation – restating the problem

By utilizing a linear approximation in each on the specific elements, a direct attempt to solve the differential equation is not possible. Discontinuities arise on the common edges between elements, as base functions are not continuous between elements, hence derivatives cannot be defined on the edges. A weaker formulation must be then used for solving the differential equation, where a solution is needed that is in average satisfied in the domain. Let $L\varphi=g$ a differential equation, where L is a differential operator, φ is the unknown function and g is the known stimulating function. In the Galerkin formulation the projection of the residual $R=L\varphi-g$ on any test function φ' must be zero. In particular the weighted residual $<R, \varphi'>$ must be zero. The expression $<\varphi_1,\varphi_2>$ is defined as an inner product in an infinite dimensional Hilbert space usually given by expression (2.7). The Galerkin formulation of the differential equation with the use of weighted residuals is given by equation (2.8).

$$<\varphi_1\varphi_2>=\iint_{\Omega}\varphi_1\varphi_2 ds \tag{2.7}$$

$$<L\varphi-g,\varphi'>=\iint_{\Omega}\varphi'\left(L\varphi-g\right)ds=0,\ \forall\varphi' \tag{2.8}$$

2.4 Perfectly Matched Layers (PML)

While studying electromagnetic problems, where the testing domain is infinite, boundary conditions must be utilised. Their goal is to truncate the under test domain, in order to simulate its infinite dimension without inserting variations or distortions of the electromagnetic fields. For this goal the widely used perfectly matched layers (PML) technique can be used. PML was initially proposed by Berenger [2], who inserted an artificail lossy medium that has the ability to absorb electromagnetic waves without any reflections for any frequency and incident angle. Consequently Chew *et al.* [3] provided a different formulation that was based on complex parameters of a coordinata stretching scheme. Both notations have the disadvantage of modifying the Maxwell equations. The dominating version today, particularly in FEM formulations is the scheme that was proposed by Sacks *et al.* [4]. They proposed a formulation where a diagonal anisotropic medium with all the same properties that does not insert any reflections and ther is no need to modify Maxwell's equations. The proposed medium has also the advantage of an easy incorporation to finite element techniques without substantial changes to the implemented code. Consequently a short description of the proposed by Sacks *et al.* medium in the simple case of an incident plane wave on an absorbing medium (area 2), with the medium's state parameters defined in figure 2.4.1.

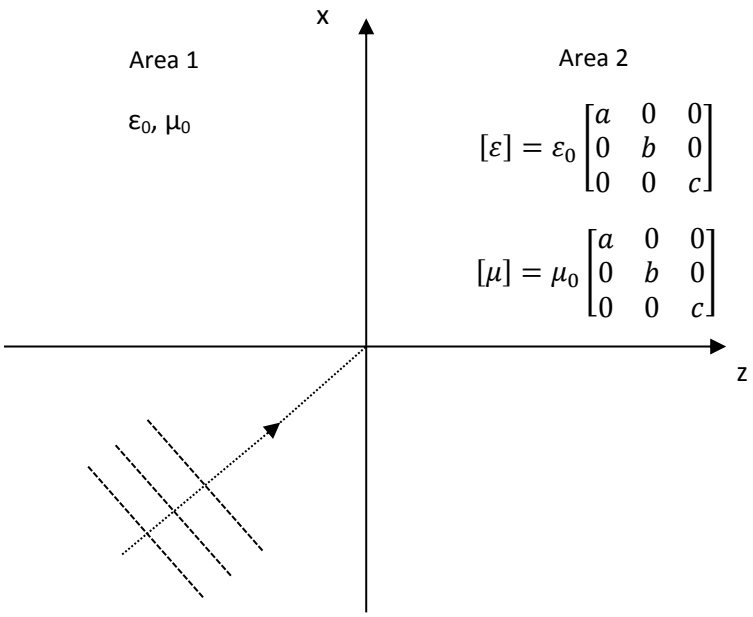

Figure 2.4.1. Incident plane wave on a PML

Necessary and sufficient condition for having only a refractive wave is matching between the two mediums characteristic impedances (equation 2.9).

$$\frac{[\varepsilon]}{\varepsilon_0} = \frac{[\mu]}{\mu_0} \tag{2.9}$$

It can be shown [4] that if the complex parameters α, b, c are defined as $a = b = 1/c$, then the reflection coefficient is zero for both TE and TM polarizations, for any incident angle and frequency. In this way PML can be characterised by one complex parameter $a = a - j\beta$, with parameter a determining the wavelength inside the diagonal anisotropic medium and parameter β determining wave attenuation. The dispersion equation of the PML is given by:

$$\frac{k_x^2}{bc} + \frac{k_y^2}{ac} + \frac{k_z^2}{ab} = k_0^2 \tag{2.10}$$

If we replace the extracted relations for the parameters a, b, c to the tensors of complex dielectric and magnetic permeability of PML, then it can be easily observed that the magnetic and electric conductivity of the medium have negative values, thus denoting the its artificial character.

In practice, the medium must be terminated by a finite plate of known refractance (usually PEC or PMC) as depicted in figure 2.4.2. Defining Q as the known

reflection coefficient of the finalizing plate, then the total refractance for the PML and the finite plate is given by equation

$$|R| = |Q| e^{-2\beta k_0 \cos\theta_i d} \tag{2.11}$$

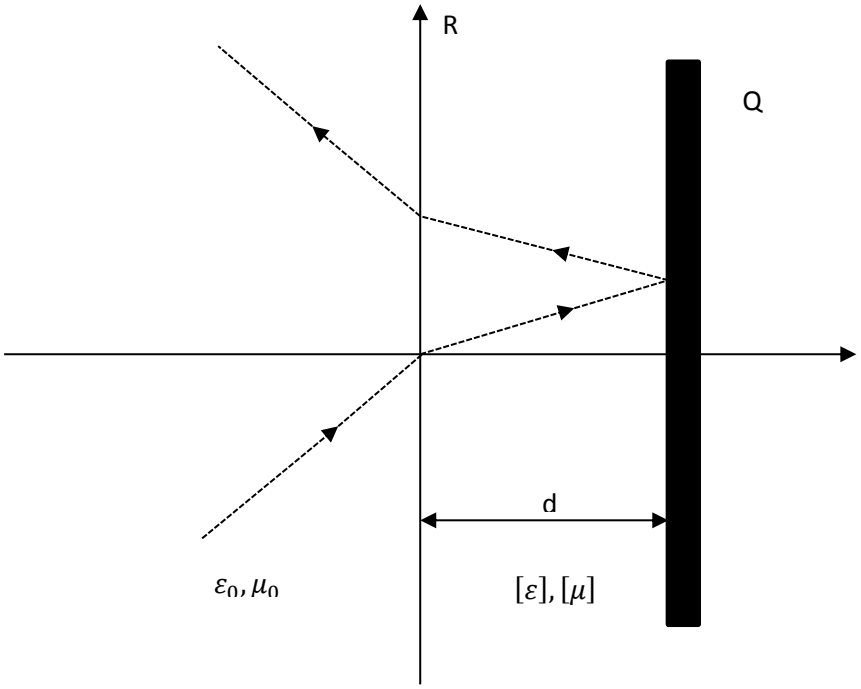

Figure 2.4.2. Reflection of a finite plate with PML

2.5 Scattering by a dielectric of an arbitrary cross section

Let's define a dielectric scatterer of an arbitrary cross section and a TM plane wave on the z axis with zero incidence angle depicted in figure 2.5.1. The electric and the magnetic field of the wave will be given by

$$\vec{\boldsymbol{E}}_i = E_0 e^{j(\omega t - k_0 x)} \hat{z} \tag{2.12}$$

$$\vec{\boldsymbol{H}}_i = \frac{E_0}{Z_0} e^{j(\omega t - k_0 x)} \hat{y} \tag{2.13}$$

When calculating the scattered and total field, around the scatterer and inside it, the finite element method has to be used due to the arbitrariness of the cross section with the infinite surrounding medium being truncated by PML layers as mentioned in section 2.4.

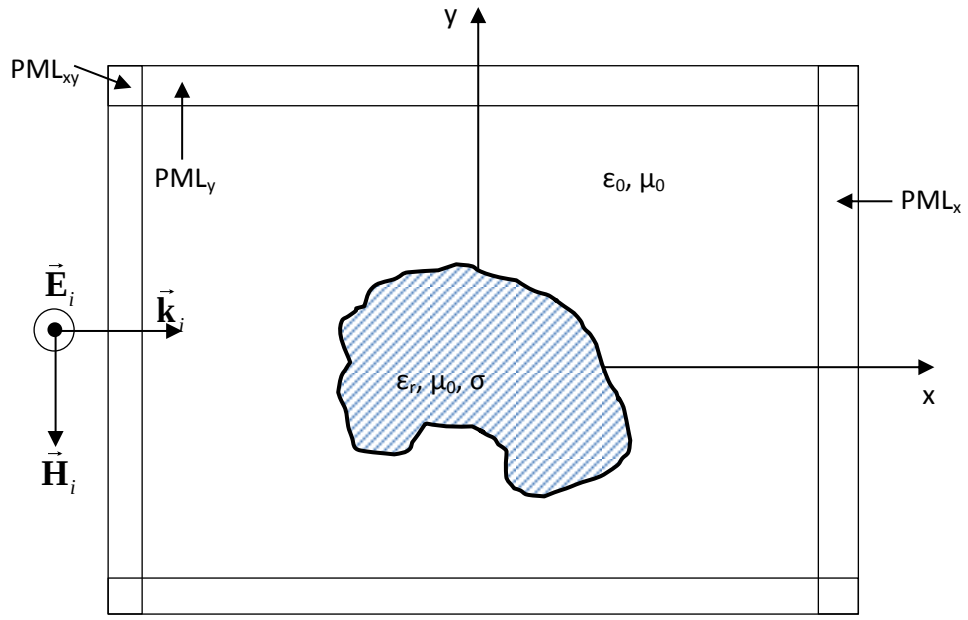

Figure 2.5.1. Scattering by dielectric of an arbitrary cross section

The scattering wave still has the same form as the incident wave; it is still a transverse magnetic (TM) wave. Total field will be defined by

$$\vec{\mathbf{E}}_{\mathbf{tot}} = \vec{\mathbf{E}}_{\mathbf{i}} + \vec{\mathbf{E}}_{\mathbf{s}} \tag{2.14}$$

$$\vec{\mathbf{E}}_{\mathbf{tot}} = E_z^i \hat{z} + E_z^s \hat{z} = E_z^{tot} \hat{z} \tag{2.15}$$

Maxwell's and Helmholtz equations apply to the problem.

$$\nabla \times \vec{\mathbf{E}}_{tot} = -j\omega \bar{\mu}_r \mu_0 \vec{\mathbf{H}}_{tot} \tag{2.16}$$

$$\nabla \times \vec{\mathbf{H}}_{tot} = -j\omega \bar{\varepsilon}_r \varepsilon_0 \vec{\mathbf{E}}_{tot} \tag{2.17}$$

$$\nabla \times \nabla \times \vec{\mathbf{E}}_i - k_0^2 \vec{\mathbf{E}}_i = 0 \tag{2.18}$$

For simplicity reason the scattered field can be denoted as $\vec{\mathbf{E}}$ and with the help of equations (2.14) – (2.18) (appendix A) the following relation can be derived.

$$\nabla \times \bar{\mu}_r^{-1} \nabla \times \vec{\mathbf{E}} - k_0^2 \bar{\varepsilon}_r \vec{\mathbf{E}} = -\nabla \times \left(\bar{\mu}_r^{-1} - \bar{1} \right) \nabla \times \vec{\mathbf{E}}_i + k_0^2 \left(\bar{\varepsilon}_r - \bar{1} \right) \vec{\mathbf{E}}_i \tag{2.19}$$

The Galerkin formulation of (2.19) is:

$$\iint_S \vec{\mathbf{E}}' \cdot \left(\nabla \times \bar{\mu}_r^{-1} \nabla \times \vec{\mathbf{E}}\right) ds - \iint_S \vec{\mathbf{E}}' \cdot k_0^2 \bar{\varepsilon}_r \vec{\mathbf{E}} ds = - \iint_S \vec{\mathbf{E}}' \cdot \left(\nabla \times \left(\bar{\mu}_r^{-1} - 1\right) \nabla \times \vec{\mathbf{E}}_i\right) ds + \iint_S \vec{\mathbf{E}}' \cdot k_0^2 \left(\bar{\varepsilon}_r - 1\right) \vec{\mathbf{E}}_i ds \quad (2.20)$$

The first integral of the left hand side of the equation and the first integral of the right hand side of equation (2.20) with the help of vector identities and the help of vector calculus theorems (appendix A) can be expressed as

$$\iint_S \vec{\mathbf{E}}' \cdot \left(\nabla \times \bar{\mu}_r^{-1} \nabla \times \vec{\mathbf{E}}\right) ds = \iint_S \nabla \times \vec{\mathbf{E}}' \cdot \bar{\mu}_r^{-1} \nabla \times \vec{\mathbf{E}} ds + \oint_{\partial S} \vec{\mathbf{E}}' \left(n \times \bar{\mu}_r^{-1} \nabla \times \vec{\mathbf{E}}\right) \cdot dl \quad (2.21)$$

$$\iint_S \vec{\mathbf{E}}' \cdot \left(\nabla \times \left(\bar{\mu}_r^{-1} - 1\right) \nabla \times \vec{\mathbf{E}}\right) ds = \iint_S \nabla \times \vec{\mathbf{E}}' \cdot \left(\bar{\mu}_r^{-1} - 1\right) \nabla \times \vec{\mathbf{E}} ds + \oint_{\partial S} \vec{\mathbf{E}}' \left(n \times \left(\bar{\mu}_r^{-1} - 1\right) \nabla \times \vec{\mathbf{E}}\right) \cdot dl \quad (2.22)$$

The cross product of the line integrals of equations (2.22) (2.23) results in a vector either pointing at x direction or at y direction. Consequently the inner product with the vector test function $\vec{\mathbf{E}}'$, parallel with $\hat{z}$ axis, results to zero. Therefore the scattering problem can be reduced in a scalar problem in which the unknown variable is the value of the electric field parallel to $\hat{z}$ axis in the nodes of the first order triangular finite elements of the problem's mesh.

The next step is to discretize the Galerkin formulation

$$\sum_{n=1}^{N_e} \iint_{\Omega_n} \nabla \times E' \bar{\mu}_r^{-1} \cdot \nabla \times E ds - \sum_{n=1}^{N_e} \iint_{\Omega_n} E' k_0^2 \bar{\varepsilon}_r E ds = - \sum_{n=1}^{N_e} \iint_{\Omega_n} \nabla \times E' \left(\bar{\mu}_r^{-1} - 1\right) \cdot \nabla \times E_i ds + \sum_{n=1}^{N_e} \iint_{\Omega_n} E' k_0^2 \left(\bar{\varepsilon}_r - 1\right) \vec{E}_i ds \quad (2.23)$$

where Ω_n is n-th element and N_e the total number of elements in the problem's mesh. During the computational implementation, each node will have a unique identity (global numbering) in the mesh. Global numbering will denote when combining the contribution of all the elements during the assembly process. In figure 2.5.2 by 1, 2, 3 local numbering is depicted for the nodes and by p, q, r global numbering of the nodes. Every term of the form of E can be described as $E = \sum_{j=1}^{3} E_j^n N_j^n$ with index n concerning the element and the base functions being described after a reasonable assumption by an equivalent relationship $E' = \sum_{i=1}^{3} E_i'^n N_i^n$.

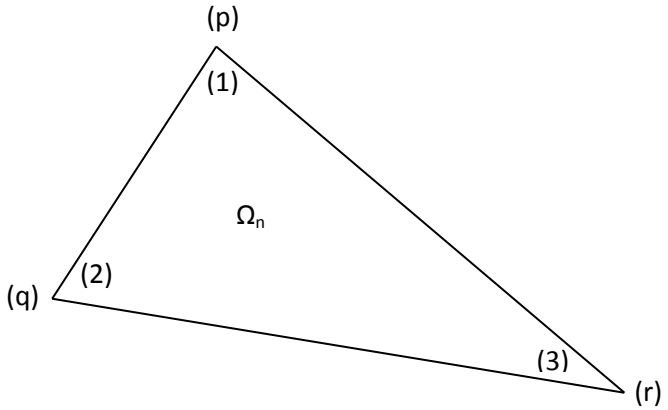

Figure 2.5.2. Nodes local and global numbering

If we look at a particular element only, equation (2.23) when utilizing the expressions that were previously mentioned and with the help of equations (2.1), (2.2), (2.5) the following equation can be derived

$$\sum_{i=1}^{3}\sum_{j=1}^{3} E_i^{'} S_{ij} E_j - k_0^2 \sum_{i=1}^{3}\sum_{j=1}^{3} E_i^{'} T_{ij} E_j = -\sum_{i=1}^{3}\sum_{j=1}^{3} E_i^{'} S_{ij}^{"} E_j^{inc} + k_0^2 \sum_{i=1}^{3}\sum_{j=1}^{3} E_i^{'} T_{ij}^{"} E_j^{inc} \tag{2.24}$$

where

$$S_{ij}^{n} = \left(c_i \mu_{r_x}^{-1} c_j + b_i \mu_{r_y}^{-1} b_j \right) A_n \tag{2.25}$$

$$S_{ij}^{"n} = \left[c_i \left(\mu_{r_x}^{-1} - 1 \right) c_j + b_i \left(\mu_{r_y}^{-1} - 1 \right) b_j \right] A_n \tag{2.26}$$

$$T_{ij}^{n} = \varepsilon_{r_z} \iint_{\Omega_n} \zeta_i \zeta_j ds \tag{2.27}$$

$$T_{ij}^{"n} = \left(\varepsilon_{r_z} - 1 \right) \iint_{\Omega_n} \zeta_i \zeta_j ds \tag{2.28}$$

with A_n the element Ω_n and b c the simplex parameters of triangle Ω_n.

The integrals of equations (2.27) (2.28) belong to the general category of simplex powers integrals on the surface of an element and can be calculating by the following analytical relation

$$\iint_{\Omega_n} \zeta_1^i \zeta_2^j \zeta_3^k ds = \frac{i!\, j!\, k!\, 2!\, A_n}{(i + j + k + 2)!} \tag{2.29}$$

The equation (2.24) can be written in the form of matrices as:

$$\left[E^{'} \right]^T \left[S_{\Omega_n} - k_0^2 T_{\Omega_n} \right] [E] = \left[E^{'} \right]^T \left[-S_{\Omega_n}^{"} + k_0^2 T_{\Omega_n}^{"} \right] \left[E^{inc} \right] \tag{2.30}$$

For solving the problem, the contribution of every single element must be taken into an account i.e. the assembly process, resulting in the following block of equations.

$$\begin{bmatrix} E_1^{1'} & E_2^{1'} & E_3^{1'} & E_1^{2'} & E_2^{2'} & E_3^{2'} & \cdots \end{bmatrix} \begin{bmatrix} S_{11}^1 - k_0^2 T_{11}^1 & S_{12}^1 - k_0^2 T_{12}^1 & S_{13}^1 - k_0^2 T_{13}^1 & & & \\ S_{21}^1 - k_0^2 T_{21}^1 & S_{22}^1 - k_0^2 T_{22}^1 & S_{23}^1 - k_0^2 T_{23}^1 & & & \\ S_{31}^1 - k_0^2 T_{31}^1 & S_{32}^1 - k_0^2 T_{32}^1 & S_{33}^1 - k_0^2 T_{33}^1 & & & \\ & & & S_{11}^2 - k_0^2 T_{11}^2 & S_{12}^2 - k_0^2 T_{12}^2 & S_{13}^2 - k_0^2 T_{13}^2 \\ & & & S_{21}^2 - k_0^2 T_{21}^2 & S_{22}^2 - k_0^2 T_{22}^2 & S_{23}^2 - k_0^2 T_{23}^2 \\ & & & S_{31}^2 - k_0^2 T_{31}^2 & S_{32}^2 - k_0^2 T_{32}^2 & S_{33}^2 - k_0^2 T_{33}^2 \\ & & & & & \end{bmatrix} \begin{bmatrix} E_1^1 \\ E_2^1 \\ E_3^1 \\ E_1^2 \\ E_2^2 \\ E_3^2 \\ \vdots \end{bmatrix}$$

$$= \begin{bmatrix} E_1^{1'} & E_2^{1'} & E_3^{1'} & E_1^{2'} & \cdots \end{bmatrix} \begin{bmatrix} -S_{11}^{"1} + k_0^2 T_{11}^{"1} & -S_{12}^{"1} + k_0^2 T_{12}^{"1} & -S_{13}^{"1} + k_0^2 T_{13}^{"1} & & \\ -S_{21}^{"1} + k_0^2 T_{21}^{"1} & -S_{22}^{"1} + k_0^2 T_{22}^{"1} & -S_{23}^{"1} + k_0^2 T_{23}^{"1} & & \\ -S_{31}^{"1} + k_0^2 T_{31}^{"1} & -S_{32}^{"1} + k_0^2 T_{32}^{"1} & -S_{33}^{"1} + k_0^2 T_{33}^{"1} & & \\ & & & -S_{11}^{"2} + k_0^2 T_{11}^{"2} & -S_{12}^{"2} + k_0^2 T_{12}^{"2} & -S_{13}^{"2} + k_0^2 T_{13}^{"2} \\ & & & -S_{21}^{"2} + k_0^2 T_{21}^{"2} & -S_{22}^{"2} + k_0^2 T_{22}^{"2} & -S_{23}^{"2} + k_0^2 T_{23}^{"2} \\ & & & -S_{31}^{"2} + k_0^2 T_{31}^{"2} & -S_{32}^{"2} + k_0^2 T_{32}^{"2} & -S_{33}^{"2} + k_0^2 T_{33}^{"2} \\ & & & & & \end{bmatrix} \begin{bmatrix} E_1^{1^{inc}} \\ E_2^{1^{inc}} \\ E_3^{1^{inc}} \\ E_1^{2^{inc}} \\ E_2^{2^{inc}} \\ E_3^{2^{inc}} \\ \vdots \end{bmatrix}$$

It can be easily observed that each node appears as an unknown as many times as the elements that belongs to. In order to formulate an system of linear independent equations, matrices known as connectivity matrices are [1]. As a result a sparse system of equations is formulated which can be written in a compact Galerkin form as:

$$\left[E^{'}\right]^T \left[S \;\; -k_0^2 T\right][E] = \left[E^{'}\right]^T \left[-S^{"} + k_0^2 T^{"}\right]\left[E^{inc}\right] \tag{2.30}$$

where the matrix $\left[S \;\; -k_0^2 T\right]$ is the total stiffness matrix of the system. It can be shown that [1] every element in the stiffness matrix that connects two interacting nodes with global numbering (p), (q), is the sum of the respective elements of the elemental stiffness matrices for the elements that the pair (p), (q) belongs. The column vector $\left[-S^{"} + k_0^2 T^{"}\right]\left[E^{inc}\right]$ is known as the system's load vector.

Last step is the definition of the test functions. Whether in our problem nodes with known field values exist, then vector E can be written as

$$E = \begin{bmatrix} E_f \\ E_p \end{bmatrix} \tag{2.31}$$

E_f denotes the nodes with unknown field values with are and E_p denotes nodes with known filed values. By inserting the assumption (2.31) in the Galerkin formulation (2.30) it's final form can be derived.

$$\begin{bmatrix} E_f^{'} \\ E_p^{'} \end{bmatrix}\begin{bmatrix} S_{ff}-k_0^2T_{ff} & S_{fp}-k_0^2T_{fp} \\ S_{pf}-k_0^2T_{pf} & S_{pp}-k_0^2T_{pp} \end{bmatrix}\begin{bmatrix} E_f \\ E_p \end{bmatrix}=\begin{bmatrix} E_f^{'} \\ E_p^{'} \end{bmatrix}\begin{bmatrix} -S_{ff}^{"}+k_0^2T_{ff}^{"} & -S_{fp}^{"}+k_0^2T_{fp}^{"} \\ -S_{pf}^{"}+k_0^2T_{pf}^{"} & -S_{pp}^{"}+k_0^2T_{pp}^{"} \end{bmatrix}\begin{bmatrix} E_f^{inc} \\ E_p^{inc} \end{bmatrix} \quad (2.32)$$

No restrictions arise when defining the test function, however the simplest approach is to implement in the above equation N_f times [1], assuming as a test function the base function of each node κόμβου (only for the nodes with unknown values). The following sparse system of equations can then determined

$$\left(S_{ff}-k_0^2T_{ff}\right)E_f+\left(S_{fp}-k_0^2T_{fp}\right)E_p=\left(-S_{ff}^{"}+k_0^2T_{ff}^{"}\right)E_f^{inc}+\left(-S_{fp}^{"}+k_0^2T_{fp}^{"}\right)E_p^{inc} \quad (2.32)$$

with the final system of equations having the form $\mathbf{A}X=\mathbf{B}$. By taking into account the sparseness of matrix $\mathbf{A}$, the solution of the system is possible without calculating the inverse. It must be noted that while creating the right member of the equation (2.33) it is not binding to multiply a matrix with a column vector. Finally it must be noted that in PML areas it makes no sense to impose excitation, as their purpose is to absorb waves for simulating the infinite space, thus in the right hand side of (2.32) is zero.

3. SOLVING INVERSE PROBLEMS

3.1 Inverse problem

Inverse problem can be defined as a process of exporting the physical parameters of a system by its response. Inverse problems which can be cast as optimization problems can be found in many different occasions such as electromagnetic scattering, tomography image reconstruction and remote sensing. For instance, during satellite mapping of an area the acquired signal is the voltage of the satellite sensors. By the variations of the voltage information whether the area is characterised by dense vegetation, water tanks such as lakes, seas, or residential areas can be derived.

Inverse problems are characterised as ill-posed problems [5], i.e. problems that if we accept the existence of a solution, its independence form system response and uniqueness cannot be proved. For instance, let's consider two electromagnetic sources that do not radiate out of a certain area. As a result these two sources cannot be detected out of this specific area. The existence of two different sources that radiate the same far field is also possible. For example two spherical sources of different radius radiating at the same frequency such that the received phase is equal at a certain distance for an observer. These two sources are indistinguishable at that point. Even if we accept the uniqueness of the solution the stability must be checked. An occurring small variation in the input data should not lead to dramatic changes in the solution of the inverse problem. Such an assumption is not valid for inverse problems since they are mostly nonlinear.

Solving inverse problems is a process that is usually performed through nonlinear optimization-regularization techniques, which are usually iterative [5, 6, 12, 13, 15]. These procedures with the use of different algorithms select one of the infinite possible solutions and stabilize it so any input noise will not lead to extreme variations in the problems solution. Another approach for solving inverse problems is the attempt to linearize them; however such techniques as of today cannot achieve an adequate solution in those cases that quantitative reconstruction of an object is desirable.

3.2. Microwave Tomography (MWT)

Microwave tomography, an inverse electromagnetic scattering problem, is a quantitative imaging technique of dielectric properties of an unknown object with applications in non-destructive testing, biomedical purposes, geophysical research, through the wall imaging and security scanners. The unknown object that is to be depicted (*object of interest-OI*), that is enclosed by a medium with known dielectric properties (*background medium*), is illuminated consecutive by electromagnetic sources, which are located in different positions. The scattered fields emerging from the different sources are measured at different positions around the OI (figure 3.5.1). Through those measured scattered electromagnetic fields the reconstruction of the dielectric properties of the OI is performed.

The problem of microwave tomography is nonlinear since both the dielectric properties of the OI and the electromagnetic fields inside the OI are unknown. However it comprises a rather promising technique especially in biomedical applications since:

- it is characterised by low cost and portability especially in comparison with magnetic resonance imaging (MRI),
- it uses safe non ionizing radiation compared to X-ray imaging which according to recent research results from the USA National Cancer Institute, rays of 60 mGy can increase the probability of brain cancer or leukemia by three times in children below 10 years old [11],
- has the ability to picture the dielectric properties as a tissue characteristic, something that is not possible in any other imaging modality,
- it can quantitatively reconstruct the frequency dependent dielectric properties and the conductivity of living tissue, as a method to identify its physiology.

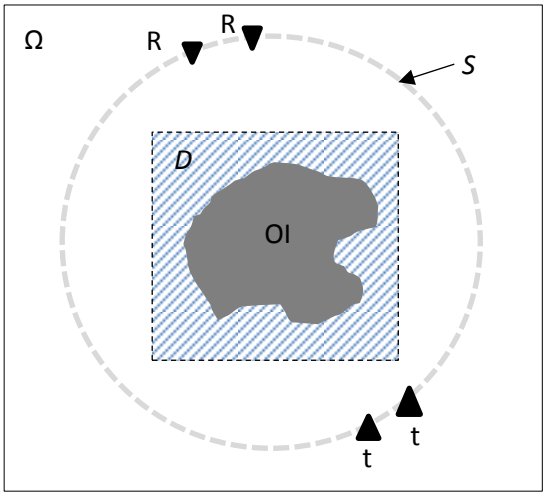

Figure 3.2.1. Geometric representation of MWT, *D* is the imaging domain, *S* the measuring surface, Ω total domain of the problem, *R* receivers, *t* sources

3.3 Mathematical formulation of inverse electromagnetic scattering

It is known that [7] in an inhomogeneous anisotropic medium the following relations apply

$$\nabla\times\bar{\mu}_r^{-1}\nabla\times\mathbf{E}-k_0^2\bar{\varepsilon}_r^*(\mathbf{r},\omega)\mathbf{E}=-j\omega\mu_0\mathbf{J}(\mathbf{r},\omega) \tag{3.1}$$

$$\nabla\times\bar{\mu}_r^{-1}\nabla\times\mathbf{E}^{inc}-k_0^2\bar{\varepsilon}_{r_b}^*(\mathbf{r},\omega)\mathbf{E}^{inc}=-j\omega\mu_0\mathbf{J}(\mathbf{r},\omega) \tag{3.2}$$

$$\mathbf{E}=\mathbf{E}^S+\mathbf{E}^{inc} \tag{3.3}$$

where $\bar{\varepsilon}_r^*(\mathbf{r},\omega)$ is the relative complex permittivity and $\bar{\varepsilon}_{r_b}^*(\mathbf{r},\omega)$ is the relative complex permittivity of the background medium.

Subtracting equations (3.1) (3.2) and with the help of (3.3) we end in equation

$$\nabla\times\bar{\mu}_r^{-1}\nabla\times\mathbf{E}^S-k_0^2\bar{\varepsilon}_{r_b}^*(\mathbf{r},\omega)\mathbf{E}^S=k_0^2\bar{\varepsilon}_{r_b}^*\frac{\bar{\varepsilon}_r^*-\bar{\varepsilon}_{r_b}^*}{\bar{\varepsilon}_{r_b}^*}\mathbf{E}$$

The contrast χ terns (zero outside the scatterer) and contrast source w are defined as

$$\chi(\mathbf{r},\omega)=\frac{\bar{\varepsilon}_r^*-\bar{\varepsilon}_{r_b}^*}{\bar{\varepsilon}_{r_b}^*} \tag{3.4}$$

$$w=\chi(\mathbf{r},\omega)\mathbf{E} \tag{3.5}$$

With the help of the two above definitions we end up in relation (3.6), a Helmholtz equation that correlates the unknown scattered field with the background medium.

$$\nabla\times\bar{\mu}_r^{-1}\nabla\times\mathbf{E}^S-k_0^2\bar{\varepsilon}_{r_b}^*(\mathbf{r},\omega)\mathbf{E}^S=k_0^2\bar{\varepsilon}_{r_b}^*\mathbf{w} \tag{3.6}$$

The solution [8] of equation 3.6 that denotes the *data equation* is

$$\mathbf{E}^S(\mathbf{r})=k_b^2\int_D G(\mathbf{r}',\mathbf{r})\chi(\mathbf{r}',\omega)\mathbf{E}(\mathbf{r}',\omega)dv=G_S\chi\mathbf{E},\quad \mathbf{r}\in S \tag{3.7}$$

while the total field in the domain D is given by the *domain equation* (3.8)

$$\mathbf{E}(\mathbf{r})=\mathbf{E}^{inc}+k_b^2\int_D G(\mathbf{r}',\mathbf{r})\chi(\mathbf{r}',\omega)\mathbf{E}(\mathbf{r}',\omega)dv=\mathbf{E}^{inc}+G_D\chi\mathbf{E},\quad \mathbf{r}\in D \tag{3.8}$$

with the term $G(\mathbf{r}',\mathbf{r})$ denoting the Green function of the background medium. It must be noted that both χ and $\mathbf{E}$ terms are unknown.

The most common way of solving inverse scattering problems is the formulation of a cost functional and the attempt to minimize it. In every case the inversion method must minimize the error of the data equation

$$F(\omega) = \left\| \mathbf{E}^S - G_S(\omega) \right\|_S^2 \tag{3.9}$$

where $\|a\|_S^2$ is the L_2-norm over the measuring surface S, which can be determined as

$$\|a\|_S^2 = \langle a, a \rangle_S = \int_S a(\mathbf{r}) \overline{a(\mathbf{r})} d\mathbf{r} \tag{3.10}$$

with the bar over α representing the complex conjugate. In almost all inversion methods an attempt is made to minimize equation (3.9), however due to the ill-posed nature of the problem a direct simple attempt to minimize it would lead to incorrect results. The ill-posed character of the problem can also be expressed as the existence of infinite local minima that satisfy the minimization relation, with the starting point of the algorithm playing a substantial role in the selection of one of the minima. For all the aforementioned reasons it is essential to conduct some sort of regularization, that has to do with a selection from one of the infinite possible solutions and stabilize the method so that reasonable variations in the input data would be suppressed and lead to the same result.

It should be explained here the term of *inverse crime* [12, 13] that is encountered very often in the literature of inverse problem solving. Inverse crime arises during the evaluation of an inversion algorithm when synthetic measurement datasets are used (*forward*) which comes from a similar solver with the one used in the inversion method (*inverse*). Such an approach tends to lead to better results thus not having a clear image of the validity of the inversion algorithm. More specifically inverse crime arises when the discretization of the domain and the model (2D TM) for creating the synthetic measurements is the same with the one used in the inversion process. In order to avoid inverse crime a different discretization can be used on the two solvers, forward and inverse, as well as the addition of artificial noise to the synthetic data.

3.4 Contrast Source Inversion (CSI) Method

One method of nonlinear minimization and regularization for solving inverse electromagnetic scattering problems that takes into account the physics of the problem at hand is contrast source inversion (CSI) [8, 9, 10, 14]. It is capable of providing quantitative results from measurements in some or even a single frequency without the use of a forward solver. A cost functional based on the scattered fields outside the OI and the total field inside the OI is used. The CSI method's advantage is its ability, apart from quantitative reconstruction of dielectric properties of the OI, to provide

information for the solution of the clinical classification problem (healthy or unhealthy tissue), regarding it as suitable for biomedical applications. The only way of minimization until today is through iterative procedures that are based on modified gradient techniques. It is formed in a way that any necessary form of regularization is implemented automatically and does not require the presence of a forward solver in each iteration. The nonlinearity of the method however leads to mathematical complexity that in turn leads to higher computational requirements for the solution of the inverse problem.

In the CSI method the cost functional has variables the terms of contrast and contrast source

$$F(\chi, w_t) = F^S\left(w_t\right) + F^D\left(\chi, w_t\right) = \frac{\sum_t \left\| \tilde{E}_t^S - G_S\left(w_t\right) \right\|_S^2}{\sum_t \left\| \tilde{E}_t^S \right\|_S^2} + \frac{\sum_t \left\| \chi \mathrm{E}_t^{inc} - w_t + \chi G_D\left(w_t\right) \right\|_D^2}{\sum_t \left\| \chi \mathrm{E}_t^{inc} \right\|_D^2} \tag{3.11}$$

Our goal is to minimize the cost functional through two interdigitated sequences of unknown variables. The first sequence corresponds to the contrast χ_n terms, which are related with the contrast source w_n terms. Index *n* denotes the iteration of the procedures and index *t* denotes the different electromagnetic excitation sources. For every iteration the contrast source terms are updated through a conjugated gradient technique [16] with the contrast regarded as a constant. Consequently, by minimizing the domain equation contrast terms are updated. The iterative procedure continues until a desirable minimum is achieved. Finally it must be noted that the term $\tilde{E}_t^S$ refers to the measured scattered fields that resulted by the excitation of the source t.

In order to provide further details about the algorithm of the iterative procedure, the *data error* term is introduced

$$\rho_{t,n} = \tilde{E}_t^S - G_S\left(w_{t,n}\right) \tag{3.120}$$

the *domain error*

$$r_{t,n} = \chi_n \mathrm{E}_t^{inc} - w_{t,n} + \chi_n G_D\left(w_{t,n}\right) \tag{3.13}$$

as well as the regularization terms

$$\eta_S = \left(\sum_t \left\| \tilde{E}_t^S \right\|_S^2 \right)^{-1}, \quad \eta_{D,n} = \left(\sum_t \left\| \chi_{n-1} \mathrm{E}_t^{inc} \right\|_D^2 \right)^{-1} \tag{3.14}$$

By regarding that the CSI method has already been initiated, the values w_{n-1}, χ_{n-1} are known, hence for the update of the contrast source term the following equation can be implemented.

$$w_{t,n} = w_{t,n-1} + a_{t,n} d_{t,n} \tag{3.15}$$

where $a_{t,n}$ is the step update for every source in the n-th iteration and $d_{t,n}$ are the Polak-Ribière directions over which the minima are being searched.

For the Polak-Ribière directions the following relation applies

$$d_{t,n} = -g_{t,n} + \frac{\langle g_{t,n}, g_{t,n} - g_{t,n-1} \rangle_D}{\|g_{t,n-1}\|_D^2} d_{t,n-1}, \quad d_{t,0} = 0, \quad n \geq 1 \tag{3.16}$$

As $g_{t,n}$ the derivatives of the cost functional corresponding to $w_{t,n}$ are defined, calculated at $w = w_{t,n-1}$ $\chi = \chi_{n-1}$ and given by the expression:

$$g_{t,n} = -\eta_S G^{S*} \rho_{t,n-1} - \eta_{D,n} \left[r_{t,n-1} - G^{D*} \left(\bar{\chi}_{n-1} r_{t,n-1} \right) \right] \tag{3.17}$$

$$G_S^* \rho_{t,n-1} = \overline{k_b^2} \int_S \overline{G(\mathbf{r}, \mathbf{r}')} \rho_{t,n-1}(\mathbf{r}') dv, \quad \mathbf{r} \in D \tag{3.18}$$

$$G_D^* \left(\bar{\chi}_{n-1} r_{t,n-1} \right) = \overline{k_b^2} \int_D \overline{G(\mathbf{r}, \mathbf{r}')} \left(\bar{\chi}_{n-1} r_{t,n-1} \right)(\mathbf{r}') dv, \quad \mathbf{r} \in D \tag{3.19}$$

Having fully setting the Polak-Ribière directions the only thing that has yet to be determined is the calculation of the step update, which can be done by minimizing the following equation

$$F_n = \eta_S \sum_t \left\| \rho_{t,n-1} - a_{t,n} G^S \left(d_{t,n} \right) \right\|_S^2 + \eta_D \sum_t \left\| r_{t,n-1} - a_{t,n} \left\{ d_{t,n} + \chi_{n-1} G^D \left(d_{t,n} \right) \right\} \right\|_D^2 \tag{3.20}$$

By setting $\partial F_n / \partial a = 0$ we end up with the final equation (3.21) of the step update

$$a_{t,n} = \frac{-\langle g_{t,n}, d_{t,n} \rangle_D}{\eta_S \left\| G^S \left(d_{t,n} \right) \right\|_S^2 + \eta_{D,n} \left\| d_{t,n} - \chi_{n-1} G^D \left(d_{t,n} \right) \right\|_D^2} \tag{3.21}$$

The update procedure for the contrast sources w having been fully derived the update procedure of the contrast χ must also be noted.

In each iteration contrast χ is updated after having updated the contrast source w. The update is utilized through minimization of the cost functional (3.11) corresponding to χ, regarding w as constant and assuming that the term η_D is independent of χ. Thus the following equation can be extracted:

$$\chi_n = \frac{\sum_t w_{t,n} \bar{E}_{t,n}}{\sum_t |E_{t,n}|} \tag{3.22}$$

What yet has to be determined is the selection of the initial values for the contrast and contrast source. A random initial χ_0 can be selected from which the initial contrast source w_0 can be derived. The typical method for calculating the initial values is to initialize our method by trying to minimize the *data equation*

$$F^S\left(w_t\right)=\left\|\tilde{E}_t^S-G^S\left(w_t\right)\right\|_S^2 \tag{3.23}$$

Basically it can be regarded as a back-propagation technique, thus arriving in the following equation

$$w_{t,0}=\frac{\left\|G^{S*}\tilde{E}_t^S\right\|_D^2}{\left\|G^S G^{S*}\tilde{E}_t^S\right\|_S^2}G^{S*}\tilde{E}_t^S \tag{3.24}$$

Next with the help of equation (3.22) the initial contrast value χ_0 can be calculated.

3.5 FEM-CSI Method

Integral equation and Green function formulations in inversion problems, in spite the fact that having been developed first, have some notables disadvantages. In integral equation formulation the calculation of the background medium's Green function is rather dire and elaborate procedure, especially in the case where the medium is inhomogeneous or the boundaries are arbitrarily shaped or conductive. Even in the case where the Green function has been fully defined, the integral equations are solved mostly with the method of moments (MoM), which on the contrary with the finite element technique leads to a dense system of equations. To overcome those hurdles while using Green functions recently the introduction of finite differences technique (FDTD) in the CSI method was suggested [14]. However still some drawbacks arise, since the technique is difficultly implemented in arbitrarily shaped boundaries due to the uniform discretization grid used in finite difference implementations. Furthermore, in rectangular grids obstacles arise when *a-priori* information is to be incorporated for the dielectric properties during the inversion algorithm.

A FEM discretization in an inversion problem can easily overcome the aforementioned hurdles providing the ability of mesh refinement only in certain areas to increase resolution keeping computational complexity to a minimum. Quite recently [17] the FEM-CSI method has been proposed, which tries to combine the advantages of the finite element discretization and the CSI method. Although inversion methods based on finite element formulations have been proposed earlier [18, 19], they had the drawback of rewriting the FEM equations at the end of each iteration of the method. This complication and be easily suppressed with the use of the CSI method.

Following the process explained in chapter 2 and the explanation of appendix A, by discretizing the equation (3.6) in domain Ω for the case of a TM two dimension problem the following equation can be easily derived

$$\left[\mathbf{S}-\mathbf{T}_b\right]\left[E_{t,w}^{S}\right]=\mathbf{T}_b w_{t,\Omega} \tag{3.25}$$

S and T_b are NxN dimension matrices, where N is the number of nodes in the domain Ω and depend on the properties of the background medium. Matrices $E_{t,w}^{S}$ and $w_{t,\Omega}$ are of $Nx1$ dimension and contain the values of the scattered fields and the values of contrast source respectively, in the domain nodes for the excitation source t.

Elements $S_{i,j}$ and $T_{bi,j}$ are given by:

$$S_{i,j}=\int_{\Omega}\nabla\times N_i\cdot\mu_r^{-1}\nabla\times N_j ds \tag{3.26}$$

$$T_{b_{i,j}}=k_0^2\varepsilon_{r_{b,z}}\int_{\Omega}N_i N_j ds \tag{3.27}$$

where N are the base functions of the finite element formulation. In order to better describe the FEM-CSI method some matrix-operators must be introduced as well as the definitions of L_2-norms and inner products.

The operator $\mathbf{M}_S\in\mathbb{C}^{R\times N}$ provides the values of the measured scattered field in the R positions of the receivers, with N the number of nodes in the problem. Assuming that the receivers are placed inside the problem's domain, by interpolating with the use of base functions the scattered fields can be calculated. Hence the operator is a sparse matrix which each row has only non-zero values in the nodes of the triangle in which the receiver R belongs. The second matrix operator is $\mathbf{M}_D\in\mathbb{R}^{I\times N}$ which selects the I nodes inside the imaging domain D. In every iteration the values of the unknown contrast and contrast source inside the imaging domain D are updated, however in order to solve the FEM equations the total nodes of the problem are needed and not only those inside imaging domain D. Thus it is necessary to use the transpose operator $\mathbf{M}_D^T$ which gives us the values of contrast in the total domain Ω.

$$w_{t,\Omega}=\mathbf{M}_D^T w_t \tag{3.30}$$

By incorporating the above operators in equation (3.25) a new operator $\mathbf{L}\in\mathbb{C}^{N\times I}$ can be defined, which provide the solution for the scattered fields as

$$E_{t,\Omega}^{S}=\mathbf{L}\left[w_t\right]=\left(\mathbf{S}-\mathbf{T}_b\right)^{-1}\mathbf{T}_b\mathbf{M}_D^T\left[w_t\right] \tag{3.31}$$

Going to the definitions of the L_2-norm and inner products inside the imaging domain D they can be determined as

$$\|x\|_D^2 = x^H \mathbf{T}_D x \tag{3.32}$$

$$\langle x, y \rangle_D = y^H \mathbf{T}_D x \tag{3.33}$$

with x, y random vectors with size $I \times 1$, and the exponential H denoting the hermitian (complex conjugate) and the matrix $\mathbf{T}_D \in \mathbb{R}^{I \times I}$ a sparse load matrix particularly for the nodes inside the imaging domain D which is defined by the relation:

$$T_{D_{i,j}} = \int_D N_i N_j ds \tag{3.34}$$

By surmising that the R receivers are uniform distributed over the surface S the L_2-norm and the inner product can be defined as

$$\|x\|_S^2 = x^H x \tag{3.35}$$

$$\langle x, y \rangle_S = y^H x \tag{3.36}$$

Incorporating the above operators in the main cost functional (3.11) of the CSI method equation (3.37) can be derived

$$\begin{aligned} F(\chi, w_t) &= F^S(w_t) + F^D(\chi, w_t) \\ &= \frac{\sum_t \left\| \tilde{E}_t^S - \mathbf{M}_S \mathbf{L}[w_t] \right\|_S^2}{\sum_t \left\| \tilde{E}_t^S \right\|_S^2} + \frac{\sum_t \left\| \chi \odot \mathrm{E}_t^{inc} - w_t + \chi \odot \mathbf{M}_D \mathbf{L}[w_t] \right\|_D^2}{\sum_t \left\| \chi \odot E_t^{inc} \right\|_D^2} \end{aligned} \tag{3.37}$$

with the term $a \odot b$ referring to the Hadamard product (element wise vector or matrix product).

The data error and domain error terms are given by the equations:

$$\rho_{t,n-1} = \tilde{\mathrm{E}}_t^S - \mathbf{M}_S \mathbf{L}\left[w_{t,n-1} \right] \tag{3.37}$$

$$r_{t,n-1} = \chi_{n-1} \odot E_t^{inc} - w_{t,n-1} + \chi_{n-1} \odot \mathbf{M}_D \mathbf{L}\left[w_{t,n-1} \right] \tag{3.38}$$

Incorporating the operators does not raise any variations in the definition to the definition of Polak-Ribière directions, it varies however the definition of the derivative the derivation of which is a rather complicated process (appendix B). The derivative corresponding to the contrast is given by:

$$g_{t,n} = -2\eta_S \mathbf{T}_D^{-1} \mathbf{L}^H \mathbf{M}_S^H \rho_{t,n-1} - 2\eta_{D,n} \mathbf{T}_D^{-1} \left(\mathbf{I} - \mathbf{L}^H \mathbf{M}_D^H \mathbf{X}_{n-1}^H \right) \mathbf{T}_D r_{t,n-1} \tag{3.39}$$

where $\mathbf{I} \in \mathbb{R}^{I \times I}$ is the identity matrix and $\mathbf{X}_{n-1} = diag\left(\chi_{n-1} \right)$ is a diagonal matrix with the values of the contrast.

The step update is defined by the equation:

$$a_{t,n} = \arg\ \min_a \left\{ F\left(w_{t,n-1} + a d_{t,n}, \chi_{n-1} \right) \right\} \tag{3.40}$$

$$a_{t,n} = \frac{\eta_S \left\langle \rho_{t,n-1}, \mathbf{M}_S \mathbf{L}\left[d_{t,n} \right] \right\rangle_S + \eta_{D,n} \left\langle r_{t,n-1}, d_{t,n} - \chi_{n-1} \odot \mathbf{M}_D \mathbf{L}\left[d_{t,n} \right] \right\rangle_D}{\eta_S \left\| \mathbf{M}_S \mathbf{L}\left[d_{t,n} \right] \right\|_S^2 + \eta_{D,n} \left\| d_{t,n} - \chi_{n-1} \odot \mathbf{M}_D \mathbf{L}\left[d_{t,n} \right] \right\|_D^2} \tag{3.42}$$

Having fully completed the update process for the contrast sources with the exact same procedure as the initial CSI method, the contrast terms must be updated. This is performed by minimizing the equation:

$$F^D(\chi) = \sum_t \left\| \chi \odot \mathrm{E}_t^{inc} - w_t + \chi \odot \mathbf{M}_D \mathbf{L}\left[w_t \right] \right\|_D^2 \tag{3.43}$$

Again the contrast source terms are regarded as constants and as a result the following equation can be derived:

$$\left(\sum_t \mathbf{E}_{t,n}^H \mathbf{T}_D \mathbf{E}_{t,n} \right) \chi_n = \sum_t \mathbf{E}_{t,n}^H \mathbf{T}_D w_{t,n} \tag{3.44}$$

The $\mathbf{E}_{t,n}$ matrix is diagonal whose elements are the values of the total field inside the imaging domain, hence the vector $\mathbf{E}_{t,n} = \mathbf{E}_t^{inc} + \mathbf{M}_D \mathbf{L}\left[w_{t,n} \right]$. The derivation procedure of the equation (3.44) is given in appendix B.

The FEM-CSI method initialization is based on the same procedure as the CSI method, the data equation is under the attempt to be minimized calculating the suitable values of contrast source. The following equation is therefore derived with the exact procedure described in appendix B.

$$w_{t,0} = \frac{\mathrm{Re}\left\langle \mathbf{M}_S \mathbf{L}\left[\mathbf{G}^S \tilde{E}_t \right], \tilde{E}_t \right\rangle_S}{\left\| \mathbf{M}_S \mathbf{L}\left[\mathbf{G}^S \tilde{E}_t \right] \right\|_S^2} \mathbf{G}^S \tilde{E}_t \tag{3.45}$$

The operator $\mathbf{G}^S$ is equal with $\mathbf{G}^S = -2\eta_S \mathbf{T}_D^{-1} \mathbf{L}^H \mathbf{M}_S^H$**.** In figure 3.5.1 a brief overview of the FEM-CSI methods is given.

Construct $\mathbf{L}, \mathbf{M}_S, \mathbf{M}_D$ operators

$$\eta_S = \left(\sum_t \left\| \tilde{E}_t^S \right\|_S^2 \right)^{-1}$$

$$w_{t,0} = \frac{\mathrm{Re}\left\langle \mathbf{M}_S \mathbf{L}\left[\mathbf{G}^S \tilde{E}_t \right], \tilde{E}_t \right\rangle_S}{\left\| \mathbf{M}_S \mathbf{L}\left[\mathbf{G}^S \tilde{E}_t \right] \right\|_S^2} \mathbf{G}^S \tilde{E}_t$$

$$\left(\sum_t \mathbf{E}_{t,0}^H \mathbf{T}_D \mathbf{E}_{t,0} \right) \chi_0 = \sum_t \mathbf{E}_{t,0}^H \mathbf{T}_D w_{t,0}$$

$$\rho_{t,0} = \tilde{\mathrm{E}}_t^S - \mathbf{M}_S \mathbf{L}\left[w_{t,0} \right]$$

$$r_{t,0} = \chi_0 \odot E_t^{inc} - w_{t,0} + \chi_0 \odot \mathbf{M}_D \mathbf{L}\left[w_{t,0} \right]$$

$$d_{t,0} = 0$$

for i=1,2,...,n

$$\eta_{D,n} = \left(\sum_t \left\| \chi_{n-1} \mathrm{E}_t^{inc} \right\|_D^2 \right)^{-1}$$

$$g_{t,n} = -2\eta_S \mathbf{T}_D^{-1} \mathbf{L}^H \mathbf{M}_S^H \rho_{t,n-1} - 2\eta_{D,n} \mathbf{T}_D^{-1} \left(\mathbf{I} - \mathbf{L}^H \mathbf{M}_D^H \mathbf{X}_{n-1}^H \right) \mathbf{T}_D r_{t,n-1}$$

$$d_{t,n} = -g_{t,n} + \frac{\left\langle g_{t,n}, g_{t,n} - g_{t,n-1} \right\rangle_D}{\left\| g_{t,n-1} \right\|_D^2} d_{t,n-1}$$

$$a_{t,n} = \frac{\eta_S \left\langle \rho_{t,n-1}, \mathbf{M}_S \mathbf{L}\left[d_{t,n} \right] \right\rangle_S + \eta_{D,n} \left\langle r_{t,n-1}, d_{t,n} - \chi_{n-1} \odot \mathbf{M}_D \mathbf{L}\left[d_{t,n} \right] \right\rangle_D}{\eta_S \left\| \mathbf{M}_S \mathbf{L}\left[d_{t,n} \right] \right\|_S^2 + \eta_{D,n} \left\| d_{t,n} - \chi_{n-1} \odot \mathbf{M}_D \mathbf{L}\left[d_{t,n} \right] \right\|_D^2}$$

$$w_{t,n} = w_{t,n-1} + a_{t,n} d_{t,n}$$

$$\left(\sum_t \mathbf{E}_{t,n}^H \mathbf{T}_D \mathbf{E}_{t,n} \right) \chi_n = \sum_t \mathbf{E}_{t,n}^H \mathbf{T}_D w_{t,n}$$

$$\rho_{t,n} = \tilde{\mathrm{E}}_t^S - \mathbf{M}_S \mathbf{L}\left[w_{t,n} \right]$$

$$r_{t,n} = \chi_n \odot E_t^{inc} - w_{t,n} + \chi_n \odot \mathbf{M}_D \mathbf{L}\left[w_{t,n} \right]$$

end

Figure 3.5.1. FEM-CSI algorithm

3.6 FEM-MRCSI method

Several publications [8, 10, 14, 20, 22, 23] have proven that CSI method, in spite of its promising results, can be substantially improved with the derivation of a term of total variation *(TV)* of the reconstructed image and the attempt to minimize it. In general, a total variation regularizer penalizes contrasts with large variation from node to node as well as in contrast values that appear very noisy. The total variation term can be defined as

$$TV\left[h(\mathbf{r})\right]=\int_{D}\left|\nabla h(\mathbf{r})\right|d\mathbf{r} \tag{3.46}$$

After some attempt to incorporate the term TV [10] Van den Berg *et al.* suggested that the term could be implemented as a multiplicative one in the cost functional, thus suppressing the need of selecting a term of artificial of a weight regularizer that is necessary when implementing a TV term. By adding the multiplicative total variation term (MR), the performance of the inversion algorithm was substantially improved, leading to smoother and clearer reconstructions. The method's cost functional after the derivation of the MR term:

$$F(\chi,w_t)=F^{MR}(\chi)\left(F^{S}(w_t)+F^{D}(w_t,\chi)\right)=F^{MR}(\chi)F^{CSI}(w_t,\chi) \tag{3.47}$$

with the MR term given by the relation:

$$F_n^{MR}(\chi)=\int_{D}b_n^2(\mathbf{r})\left(\left|\nabla\chi_n(\mathbf{r})\right|^2+\delta_n^2\right)=\left\|b_n\nabla\chi\right\|_D^2+\delta_n^2\left\|b_n\right\|_D^2 \tag{3.48}$$

where

$$b_n^2(\mathbf{r})=\frac{1}{A\left(\left|\nabla\chi_{n-1}(\mathbf{r})\right|^2+\delta_n^2\right)} \tag{3.49}$$

with the term δ_n^2 having been added for ensuring differentiability between iterations and is given by the equation:

$$\delta_n^2=\frac{F_n^D\left(\chi_{n-1},w_{t,n-1}\right)}{\tilde{A}} \tag{3.50}$$

The terms A and $\tilde{A}$ are equal with the area of the imaging domain and the average area of the triangles in the mesh of finite elements respectively.

The term F_n^{MR} is based on two observations: the minimization of the error both in the domain equation and to the fact that when the term converges, it converges to one. The formulation of the new cost functional is such that in the beginning the TV

term will be minimized with a large weight since the value of the cost function is high. Furthermore the value of the cost function without the MR term is large and will continue to reduce the error in the data and domain equation as long as the TV term will reach an almost constant value very close to one. It has already been mentioned that the term δ_n^2 has been added to ensure differentiability. It has been formulated in such a way that it satisfies the following argument. Minimization of TV in the first iteration is not preferable and as the iteration index increases the TV effect should be minimized. If our data are noisy then the data error will remain at high values and as a result the weight that TV is multiplied will be greater. Therefore noise will be suppressed in every case as the need for a greater TV term in the presence of noise is automatically satisfied [8].

By incorporating the MR term the update procedure of the contrast source terms is not modified since the multiplicative term does not depend on $w_{t,n}$ and is equal to one at $\chi = \chi_{n-1}$. However the derivation of the MR term leads to variations in the update procedure of the contrast terms. During the update of the contrast terms a second update step is added through a conjugated gradient technique with the use of Polak-Ribière directions albeit that the initial value of contrast χ_n^{CSI} has been calculated in each iteration with the help of equations (3.44).

The contrast update is thus given by:

$$\chi_n^{MR} = \chi_n^{CSI} + \beta_n d_n^{\chi} \tag{3.51}$$

with the Polak-Ribière directions given by equation:

$$d_n^{\chi} = -g_n^{\chi} + \frac{\left\langle g_n^{\chi}, g_n^{\chi} - g_{n-1}^{\chi} \right\rangle}{\left\| g_{n-1}^{\chi} \right\|_D^2} d_{n-1}^{\chi}, \;\; d_0^{\chi} = 0 \tag{3.52}$$

In order to exactly calculate the Polak-Ribière directions, it is essential to define the new cost functional (3.47) derivatives corresponding to contrast terms. When trying to calculate the derivative the following equations are derived:

$$\begin{aligned} g_n^{\chi} = {} & F_n^{MR}\left(\chi_n^{CSI}\right) \frac{\partial F_n^{D}\left(\chi, w_{t,n}\right)}{\partial \chi}\bigg|_{\chi=\chi_n^{CSI}} + \\ & \left[F^{S}\left(w_{t,n}\right) + F^{D}\left(\chi_n^{CSI}, w_{t,n}\right)\right] \frac{\partial F_n^{MR}\left(\chi, w_{t,n}\right)}{\partial \chi}\bigg|_{\chi=\chi_n^{CSI}} \\ = {} & \frac{g_{MR,n}^{\chi} F^{CSI}\left(\chi_n^{CSI}, w_{t,n}\right) + g_{D,n}^{\chi} F_n^{MR}\left(\chi_n^{CSI}\right)}{\sum_t \left|E_{t,n}\right|^2} \end{aligned} \tag{3.53}$$

$$g_{MR,n}^{\chi} = -2\nabla \cdot \left(b_n^2 \nabla \chi_n^{CSI}\right) \tag{3.54}$$

$$g_{D,n}^{\chi} = 2\eta_{D,n}\sum_{t}\mathbf{T}_D^{-1}\mathbf{E}_{t,n}^{H}\mathbf{T}_D r_{t,n} \tag{3.55}$$

The term $g_{D,n}^{\chi}$ is calculated at values χ_n^{CSI}, videlicet for the values that the term is minimized, thus providing practically zero values, resulting that it can be neglected. The exact derivation procedure for the equations (3.53)-(3.55) is given in appendix C.

It can be easily understood that when calculating the Polak-Ribière directions, it is necessary to calculate the divergence of the contrast in the nodes of the problem's mesh. However in a finite element mesh a direct calculation is not possible. In spite of the fact that the base functions which are used to express the unknowns, are continuous inside each triangle, discontinuities arise on the element edges. As a result derivatives cannot be defined and the divergence calculation is not possible. Hence it is lucid to implement some form of averaging. A method [23] of calculating the divergence has been proposed, which is based on the computation of the average derivative through integration. With the help of line integrals, over a polygon with vertexes the barycenters of the triangle which the test node belongs, an approximate value of the derivative can be calculated.

The spatial derivatives imperative for calculating the term b_n^2 are easily computed for each triangle separately with the help of the base functions of each triangle by the following equation:

$$\nabla\chi^{(m)}(\mathbf{r}) = \sum_{i=1}^{3}\chi_i^{(m)}\nabla N_i^{(m)}(\mathbf{r}) = \sum_{i=1}^{3}\chi_i^{(m)}\left(b_i^{(m)}\hat{x} + c_i^{(m)}\hat{y}\right) \tag{3.56}$$

Going now to the computation of the derivatives $g_{MR,n}^{\chi}$ for each node, let's define for node i the parameter $\xi_{i,n}$ ως $\xi_{i,n} = b_{i,n}^2\nabla\chi_{i,n}$ and the parameter $\lambda_{i,n}$ according to the relation:

$$\begin{aligned}\lambda_{i,n} &= \nabla\cdot\xi_{i,n}\\ &= \nabla\cdot\left(\xi_{i,n}^{x}\hat{x} + \xi_{i,n}^{y}\hat{y}\right)\\ &= \hat{x}\cdot\nabla\xi_{i,n}^{x} + \hat{y}\cdot\nabla\xi_{i,n}^{y}\end{aligned} \tag{3.57}$$

Defining a polygon H_i as depicted in figure 3.6.1, whose vertexes are the barycenters of the triangles which node i belongs. Using vector calculus identities and the divergence theorem is can be proved [23] that the following relation applies.

$$\hat{x}\cdot\nabla\xi_{i,n}^{x} \approx \left\langle\hat{x}\cdot\nabla\xi_{i,n}^{x}(\mathbf{r})\right\rangle_{H_i} = \frac{1}{A_i}\oint_{\Gamma_i}\xi_{i,n}^{x}(\mathbf{r})\hat{x}\cdot\hat{n}\,dl_i \tag{3.58}$$

The operator $\langle\cdot\rangle_{H_i}$ provides the average value over the polygon H_i, with A_i the area of the polygon, Γ_i the line boundary of the polygon and $\hat{n}$ the outer pointing unitary vector over the boundary Γ_i.

The term $\hat{y}$ can be calculated accordingly and approximated as

$$\hat{y}\cdot\nabla\xi_{i,n}^{y} \approx \left\langle \hat{y}\cdot\nabla\xi_{i,n}^{y}(\mathbf{r})\right\rangle_{H_i} = \frac{1}{A_i}\oint_{\Gamma_i}\xi_{i,n}^{y}(\mathbf{r})\hat{y}\cdot\hat{n}\,dl_i \tag{3.59}$$

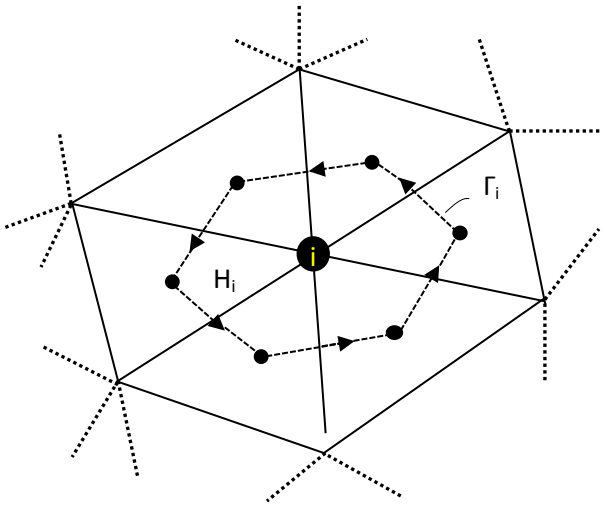

Figure 3.6.1. Polygon that surrounds the node i for the approximation of the divergence

The last step of the MR-FEMCSI methods is the determination of the step update of the contrast, which can be performed analytically through the equation

$$\beta_n = \arg\min_{real\,\beta}\left(F_n\left(w_{t,n}, \chi_n^{CSI} + \beta_n d_n^{\chi}\right)\right) \tag{3.60}$$

Equation (3.60) can be solved analytically. The cost functional is (appendix C)

$$\begin{aligned} F_n = &\left[\left\|b_n\nabla\chi_n^{CSI}\right\|_D^2 + \delta_n^2\left\|b_n\right\|_D^2 + \beta_n^2\left\|b_n\nabla d_n^{\chi}\right\|_D^2 + 2\beta_n\,\mathrm{Re}\left\langle b_n\nabla\chi_n^{CSI}, b_n\nabla d_n^{\chi}\right\rangle_D\right] \\ &\times\left[2\eta_{D,n}\beta_n\,\mathrm{Re}\sum_t\left\langle d_n^{\chi}E_t, \chi_n^{CSI}E_t - w_t\right\rangle_D + \right. \\ &\left. F^S\left(w_{t,n}\right) + F^D\left(\chi_n^{CSI}, w_{t,n}\right) + \eta_{D,n}\beta_n^2\left\|d_n^{\chi}E_t\right\|_D^2\right] \end{aligned} \tag{3.61}$$

By setting the derivative of equation (3.61) corresponding to β_n equal to zero, a third order polynomial equation is derived. Since the coefficients are all positive real numbers the roots of the equation are one real and two complex conjugate numbers. The step update of the contrast is selected as the real root of the derivative equation, since it can be proved [22] that the certain root choice does not add any local minima in the cost function, as in this case the second derivative of the cost functional is positive resulting in the existence of only one minimum. Having fully defined the update procedure of both the contrast and contrast source terms, an overview of the FEM-MRCSI inversion algorithm is given in figure 3.6.1.

Construct $\mathbf{L}, \mathbf{M}_S, \mathbf{M}_D$ operators

$$\eta_S = \left(\sum_t \left\| \tilde{E}_t^S \right\|_S^2 \right)^{-1}$$

$$w_{t,0} = \frac{\mathrm{Re}\left\langle \mathbf{M}_S \mathbf{L}\left[\mathbf{G}^S \tilde{E}_t \right], \tilde{E}_t \right\rangle_S}{\left\| \mathbf{M}_S \mathbf{L}\left[\mathbf{G}^S \tilde{E}_t \right] \right\|_S^2} \mathbf{G}^S \tilde{E}_t$$

$$\left(\sum_t \mathbf{E}_{t,0}^H \mathbf{T}_D \mathbf{E}_{t,0} \right) \chi_0 = \sum_t \mathbf{E}_{t,0}^H \mathbf{T}_D w_{t,0}$$

$$\rho_{t,0} = \tilde{\mathrm{E}}_t^S - \mathbf{M}_S \mathbf{L}\left[w_{t,0} \right]$$

$$r_{t,0} = \chi_0 \odot E_t^{inc} - w_{t,0} + \chi_0 \odot \mathbf{M}_D \mathbf{L}\left[w_{t,0} \right]$$

$$d_{t,0} = 0,\ d_0^{\chi} = 0$$

for i=1,2,...,n

$$\eta_{D,n} = \left(\sum_t \left\| \chi_{n-1} \mathrm{E}_t^{inc} \right\|_D^2 \right)^{-1}$$

$$g_{t,n} = -2\eta_S \mathbf{T}_D^{-1} \mathbf{L}^H \mathbf{M}_S^H \rho_{t,n-1} - 2\eta_{D,n} \mathbf{T}_D^{-1} \left(\mathbf{I} - \mathbf{L}^H \mathbf{M}_D^H \mathbf{X}_{n-1}^H \right) \mathbf{T}_D r_{t,n-1}$$

$$d_{t,n} = g_{t,n} + \frac{\left\langle g_{t,n}, g_{t,n} - g_{t,n-1} \right\rangle_D}{\left\| g_{t,n-1} \right\|_D^2} d_{t,n-1}$$

$$a_{t,n} = \frac{\eta_S \left\langle \rho_{t,n-1}, \mathbf{M}_S \mathbf{L}\left[d_{t,n} \right] \right\rangle_S + \eta_{D,n} \left\langle r_{t,n-1}, d_{t,n} - \chi_{n-1} \odot \mathbf{M}_D \mathbf{L}\left[d_{t,n} \right] \right\rangle_D}{\eta_S \left\| \mathbf{M}_S \mathbf{L}\left[d_{t,n} \right] \right\|_S^2 + \eta_{D,n} \left\| d_{t,n} - \chi_{n-1} \odot \mathbf{M}_D \mathbf{L}\left[d_{t,n} \right] \right\|_D^2}$$

$$w_{t,n} = w_{t,n-1} + a_{t,n} d_{t,n}$$

$$\left(\sum_t \mathbf{E}_{t,n}^H \mathbf{T}_D \mathbf{E}_{t,n} \right) \chi_n^{CSI} = \sum_t \mathbf{E}_{t,n}^H \mathbf{T}_D w_{t,n}$$

$$g_n^{\chi} = \frac{-2F^{CSI}\left(\chi_n^{CSI}, w_{t,n} \right) \nabla \cdot \left(b_n^2 \nabla \chi_n^{CSI} \right)}{\sum_t \left| E_{t,n} \right|^2}$$

$$d_n^{\chi} = g_n^{\chi} + \frac{\left\langle g_n^{\chi}, g_n^{\chi} - g_{n-1}^{\chi} \right\rangle}{\left\| g_{n-1}^{\chi} \right\|_D^2} d_{n-1}^{\chi}$$

$$\beta_n = \arg\min_{real\,\beta} \left(F_n \left(w_{t,n}, \chi_n^{CSI} + \beta_n d_n^{\chi} \right) \right)$$

$$\chi_n^{MR} = \chi_n^{CSI} + \beta_n d_n^{\chi}$$

$$\rho_{t,n} = \tilde{\mathrm{E}}_t^S - \mathbf{M}_S \mathbf{L}\left[w_{t,n} \right]$$

$$r_{t,n} = \chi_n \odot E_t^{inc} - w_{t,n} + \chi_n \odot \mathbf{M}_D \mathbf{L}\left[w_{t,n} \right]$$

end

Figure 3.6.1. FEM-MRCSI algorithm

3.7 Local minima – convergence of the CSI

As it has already been aforementioned, inverse problems greater of one dimension can only be solved through iterative procedures, since as of today no known analytical solution can be derived. Iterative procedures which are used however have a few vaguenesses one of which the point of convergence. The same applies for the CSI method, in spite of converging to adequate results whether one tries to mathematically examine the process the convergence properties are still unknown.

All the versions of the CSI method that have been presented above were based on the principle of minimizing the different variations of the cost functional, the data and the domain errors. Therefore, the problem of finding a global minimum arises whether it exists and is unique. Due to the sheer amount of unknowns and the non-linearity of the problem, a direct computation technique for the calculation of the global minima is not suitable. Thus the computation must be performed through derivatives which however have the risk of being trapped in some false local minimum. Hence it is reasonable to investigate the basic CSI method corresponding to the probability of being trapped in a certain local minimum, which is applicable for all the variations of the method that have been presented.

If we assume that the variables w_t^{exact}, χ^{exact} provide the exact solution to the inverse problem, then the contrast and contrast source terms that arise from the CSI solution procedure, can be expressed as a linear combination of the exact solution and a certain variation

$$\begin{pmatrix} w_1 \\ w_2 \\ . \\ . \\ . \\ \chi \end{pmatrix} = \begin{pmatrix} w_1^{exact} \\ w_2^{exact} \\ . \\ . \\ . \\ \chi^{exact} \end{pmatrix} + \gamma \begin{pmatrix} \Delta w_1 \\ \Delta w_2 \\ . \\ . \\ . \\ \Delta\chi \end{pmatrix} \tag{3.62}$$

Without the loss of generality the parameter γ can be regarded as a real positive number. By incorporating equation (3.62) into (3.11) a forth order polynomial is derived

$$F(\chi, w_t) = \gamma^2 \left(\mathrm{A}_D \gamma^2 + 2B_D \gamma + C_S + C_D \right) \tag{3.63}$$

$$A_D = \eta_D \sum_t \left\| \Delta\chi G_D \Delta\omega_t \right\|_D^2 \tag{3.64}$$

$$B_D = \eta_D \, \mathrm{Re} \sum_t \left\langle \Delta\chi G_D \Delta\omega_t, \Delta\chi \mathrm{E}_t^{exact} - \Delta\omega_t + \chi^{exact} G_D \Delta\omega_t \right\rangle_D \tag{3.65}$$

$$C_D = \eta_D \sum_t \left\| \Delta\chi \mathrm{E}_t^{exact} - \Delta\omega_t + \chi^{exact} G_D \Delta\omega_t \right\|_D^2 \tag{3.66}$$

$$C_S = \eta_S \sum_t \left\| G_S \Delta w_t \right\|_S^2 \tag{3.67}$$

For a specific variation and taking into account that the derivative of equation (3.63) corresponding to γ is a third order equation, 2 minima arise, a local and a global one. A sufficient condition for only one global minimum arise $(\gamma = 0)$ is

$$\frac{B_D^2}{A_D \left(C_S + C_D \right)} < \frac{8}{9} \tag{3.68}$$

Because of the Schwarz inequality:

$$B_D^2 \le A_D C_D \tag{3.69}$$

thus equation (3.68) can be transformed into equation:

$$\frac{C_D}{C_S + C_D} < \frac{8}{9} \tag{3.70}$$

When the term $\Delta\omega_t$ do not radiate are thus zero, equation (3.70) cannot be satisfied. Furthermore the regularization factor C_D is greater than the factor C_S, which is possible in the first iterations of our method, equation (3.70) is again violated. For the aforementioned reason we return to equation (3.68) and try to minimize the left term of the equation as much as possible. This can be achieved by adding more excitation sources to our problem. As long as the terms $\Delta\chi G_D \Delta\omega_t$ and $\Delta\chi \mathrm{E}_t^{exact} - \Delta\omega_t + \chi^{exact} G_D \Delta\omega_t$ have different phase distributions they are mutually cancelled during summation, whereas the term C_D remains real positive and additive. Therefore it is unambiguous that by increasing the number of excitation sources the probability of being trapped in a false local minimum is decreased.

4. APPLICATIONS - RESULTS

In this chapter certain simulations and results, that were performed in order to better comprehend the aforementioned method and techniques, are presented. Particularly in all cases the scattered electric fields by different shaped scatterers were calculated with the use of FEM. Consequently the FEM-CSI and FEM-MRCSI methods were implemented in order to reconstruct the profiles. As excitation sources, point electrical sources in two dimensions were chosen, which in a three dimensional representation can be regarded as infinite line sources [24]. These sources produce a cylindrical TM wave, with the resulting electric field parallel to the axis of the source. If an infinite line source is considered as in figure 4.1 the resulting electric field is given by the equation:

$$E_z = -I_e \frac{\omega\mu}{4} H_0^{(2)}\left(k_0 \mid \rho - \rho' \mid\right) \tag{4.1}$$

where $H_0^{(2)}$ the zeroth order Hankel function of second kind.

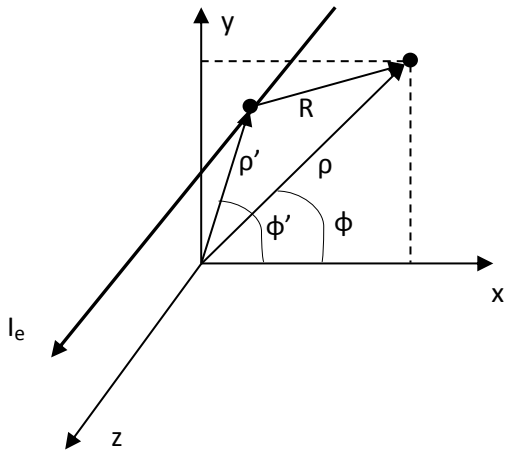

Figure 4.1. Infinite electric line source geometry

It should be noted here the criterion of choosing a TM wave. It has been proven [25] that a TE wave leads to better reconstruction results in comparison with TM waves. In order to address the TE wave two approaches can be considered, either assuming the problem as scalar corresponding to the magnetic field or the two components of the electric field on the plane transverse to the propagation direction will be regarded as the problems variables. The first approach leads to a complex mathematical formulation. Furthermore, difficulties arise when trying to model potential dielectric discontinuities

since they incorporate polarization charges which increase the non-linearity of the problem [27] and as a result tend to lead to worse results in comparison with the second approach [26]. In order to fully exploit the extra information carried by the TE polarization, both components of the electric field must be regarded as problem variables. Hence it is imperative to incorporate vector finite elements in order to avoid pseudo modes and more correct and accurate modeling of conservative vector fields. However such an approach raises the computational requirements of memory and power of the problem dramatically, since even with nodal finite elements which require a lot less memory for processing, memory requirements were at 7.2 GB. Increased requirements in computational memory arise during biomedical applications as well. Hence, due to limitations in computational power and memory, since the simulations where run on a home computer, TM polarization was selected on a two dimensional approach using nodal finite elements.

The purpose of computing the scattered electric fields was the creation of synthetic datasets so that they can be given as input data to the FEM-CSI and FEM-MRCSI methods. During the computation of the fields the domain was discretized in order the resulting triangle edges would not be greater than $\lambda/20$, so that reasonable resolution is achieved. The domain Ω was terminated with the use of PML, whose discretization was on the order of $\delta/2$, where δ the penetration depth.

Consequently, attempts to reconstruct the dielectric properties of the scatterers were performed which in all cases where paramagnetic. In order to avoid inverse crime which was explained in chapter 3 different meshes were used in the forward and inverse problem. Furthermore in the resulting electric fields noise was added according to equation:

$$\mathrm{E}_S^{noisy} = E_S + \max\left(|E_S|\right)\frac{\eta}{\sqrt{2}}\left(\tau_1 + j\tau_2\right) \tag{4.2}$$

where E_S is the measured field over the surface S which was calculated with the technique described in chapter 2, τ_1 and τ_2 are uniform distributed random variables in the interval $[-1 \quad 1]$ and η is the selected noise level which was set at $\eta = 0.05$.

During the inversion procedure the iterative algorithm was run in all cases 1024 times. Furthermore at the end of each iteration the calculated contrast was limited to results oh physical meaning. Hence the real part was set greater or equal than one and the negative part less or equal than zero.

For the validation of the algorithm's results the reconstruction error *(error)* was calculated which can be defined as

$$error = \frac{\left\| e_{r,reconstructed}(\mathbf{r}) - e_{r,exact}(\mathbf{r}) \right\|_D}{\left\| e_{r,exact}(\mathbf{r}) \right\|_D} \tag{4.3}$$

Since the two variables $e_{r,reconstructed}(\mathbf{r})$ and $e_{r,exact}(\mathbf{r})$ were defined on different triangular meshes, while calculating the error it is imperative to project the two variables on a third common rectangular grid.

4.1 U-umlaut profile

The U-umlaut profile was considered which is depicted in figures 4.1.1a 4.1.1b, whose relative dielectric permeability is equal to $\varepsilon_r = 2 - j1$. The object is placed in a background medium of $\varepsilon_{r_b} = 1$ and is illuminated by 16 different electromagnetic sources at a frequency of $f = 2GHz$. The scattered electric fields are received by 16 different receivers which are uniformly spaced over a circle of radius of 0.225m, with the sources uniformly distributed over a circle of radius 0.255m. The imaging domain D is rectangular with a side of 0.15m centered on the center of the circle of the receivers. The nodes inside the imaging domain where equal to 3618, whereas the total nodes of the problem domain Ω amount on 10506.

The scattered electric field is depicted in figures 4.1.2a 4.1.2b with the total resulting field described in figure 4.1.3a 4.1.3b. The reconstruction results with the FEM-CSI method lead to an error of 21.37% and are depicted in figures 4.1.4a and 4.1.4b. It can be observed that the reconstructed values of the relative dielectric permittivity are greater than the actual values of ε_r. Furthermore, the shape of the scatterer is not clearly reconstructed. In figure 4.1.5 the decrease of the cost functional over the number of iterations can be observed. For better supervision the cost functional value is given in logarithmic scale.

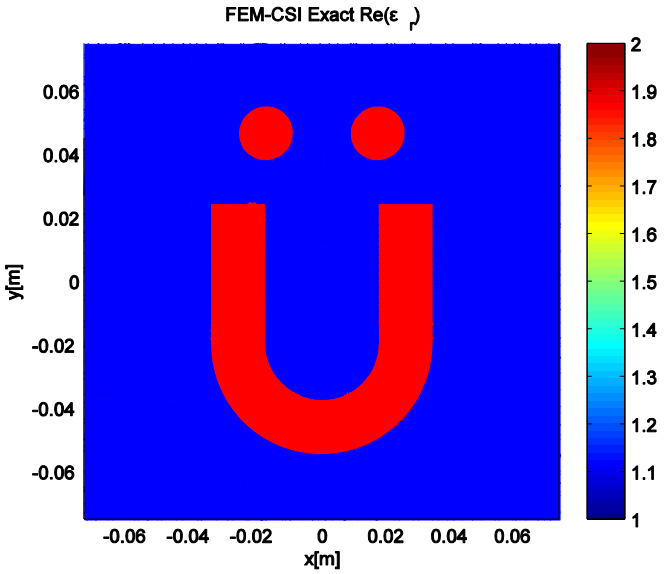

Figure 4.1.1a. Real part Re{ε_r} of relative complex permeability

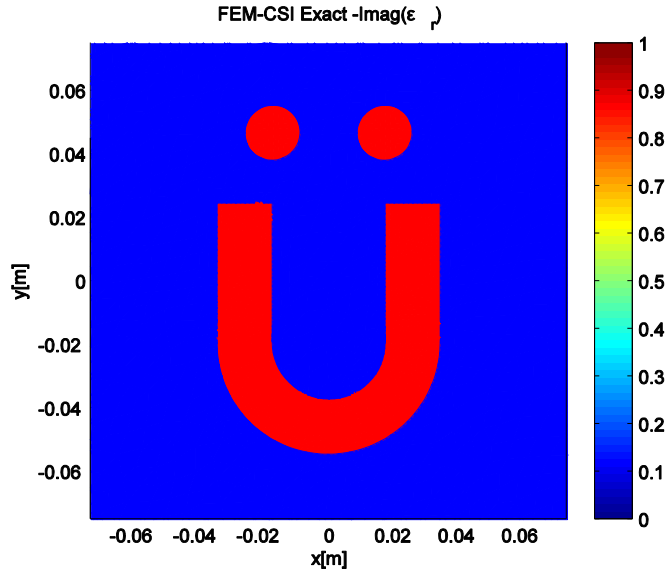

Figure 4.1.1b. Imaginary part -Im{ε_r} of relative complex permeability

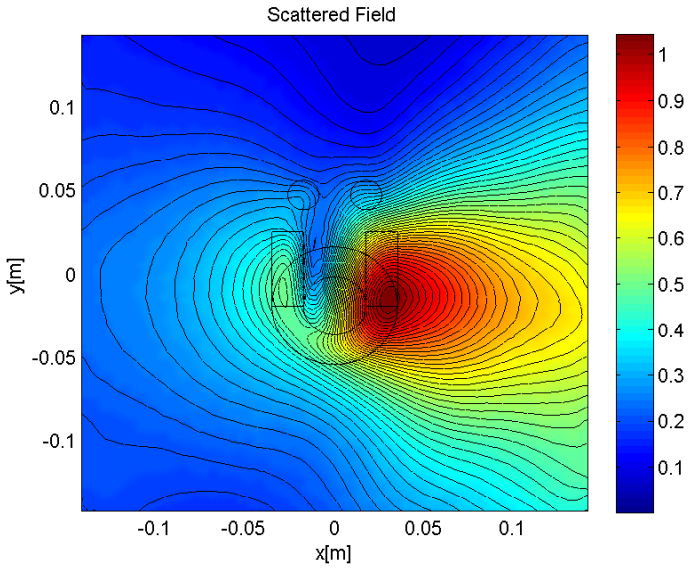

Figure 4.1.2a. Absolute value of scattered electric field with the source located at 175^o

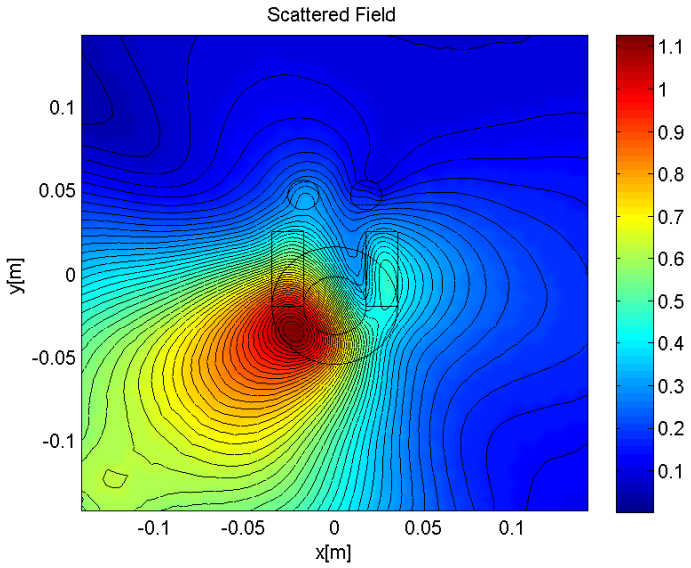

Figure 4.1.2b. Absolute value of scattered electric field with the source located at 40^o

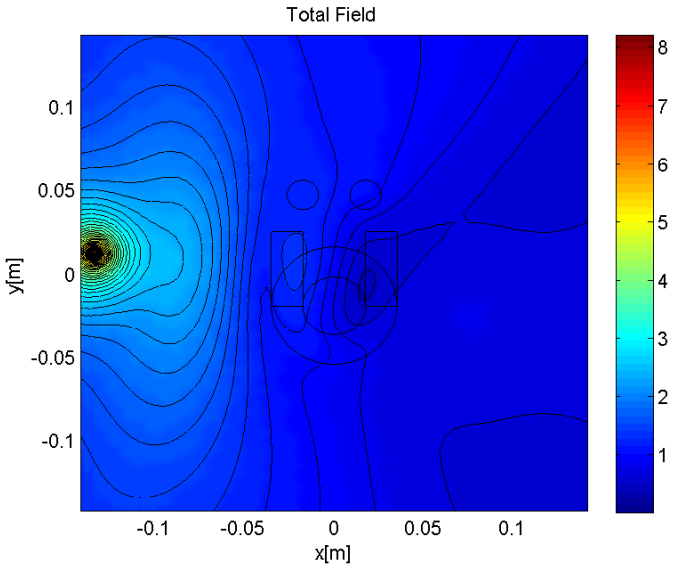

Figure 4.1.3a. Absolute value of total electric field with the source located at 175^o

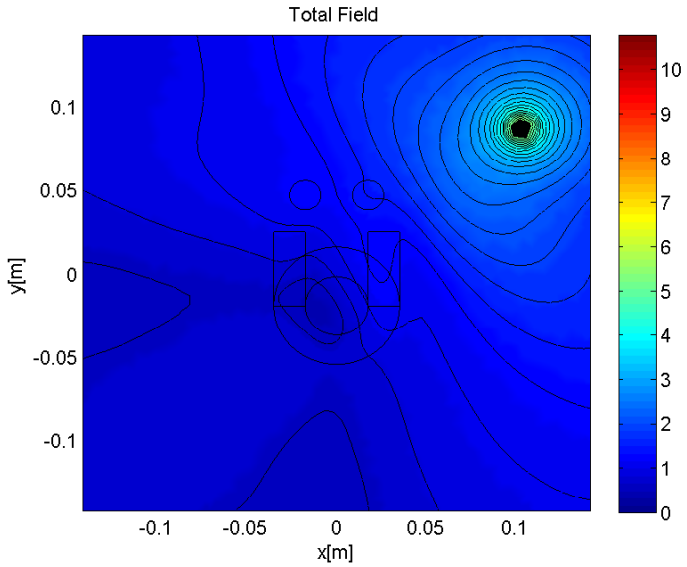

Figure 4.1.3b. Absolute value of scattered electric field with the source located at 40^o

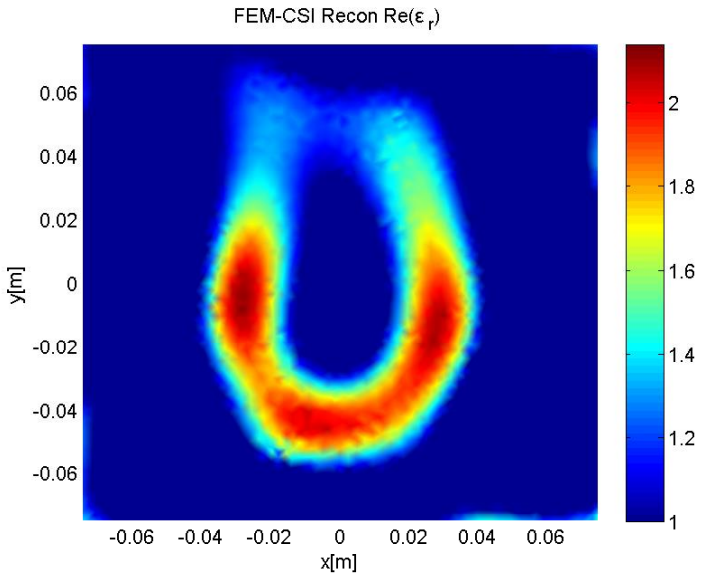

Figure 4.1.4a. Reconstructed real part Re{ε_r} of complex relative permeability

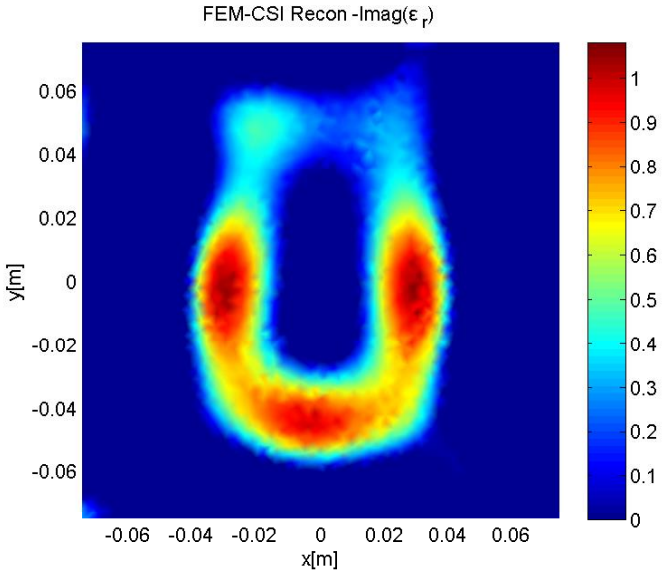

Figure 4.1.4b. Reconstructed imaginary part -Im{ε_r} of complex relative permeability

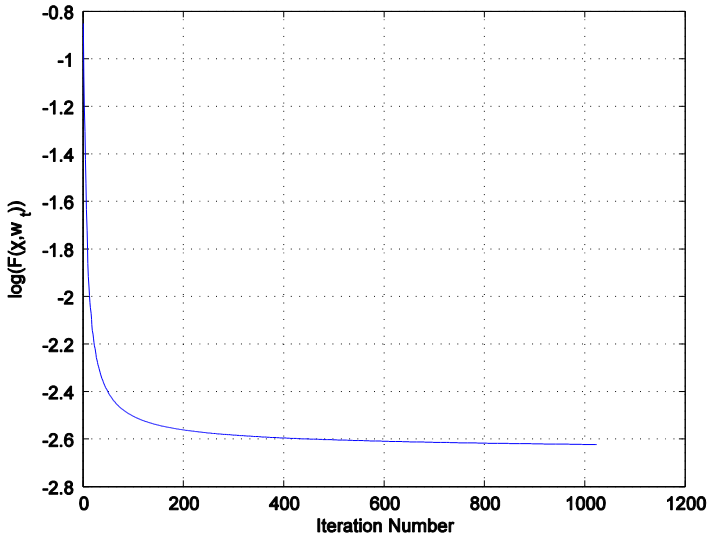

Figure 4.1.5. Cost functional

Consequently the same values of the complex permeability of the scatterer was maintained however the distance of the dots was increased. In figure 4.1.6 the imaginary part of the complex dielectric permeability is depicted in order to comprehend the exact increase of the distance, with figures 4.1.7a and 4.1.7b depicting the reconstruction results.

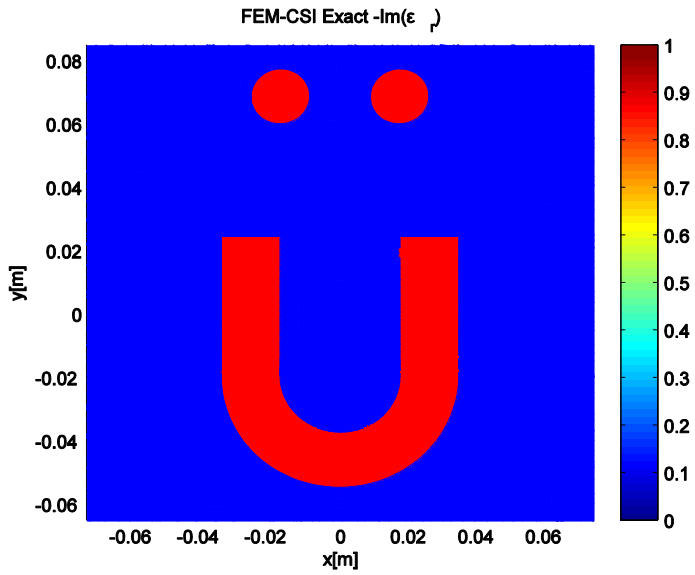

Figure 4.1.6. Imaginary part -Im{ε_r} of relative complex permeability

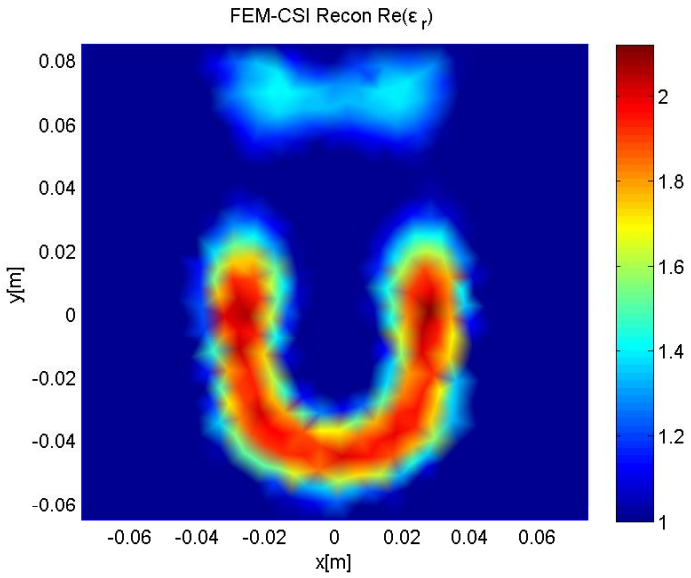

Figure 4.1.7a. Reconstructed real part Re{ε_r} of complex relative permeability

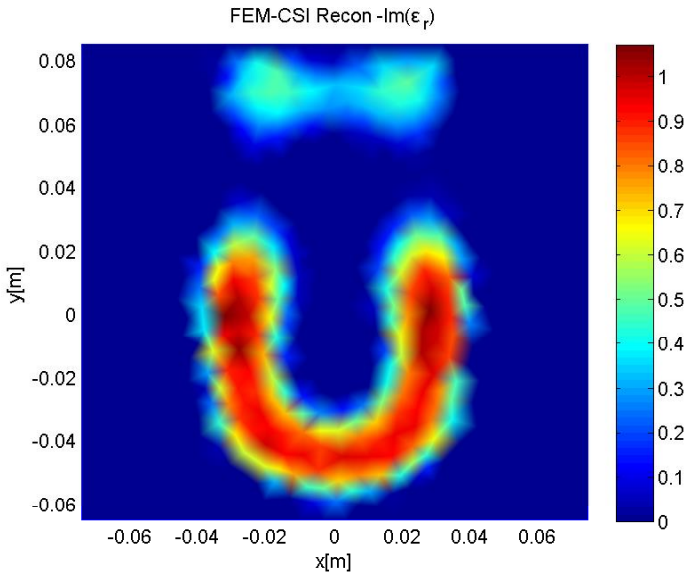

Figure 4.1.7b. Reconstructed imaginary part -Im{ε_r} of complex relative permeability

In this case the error was 18.95% and as it can be easily observed that the dots are separated clearly from the rest scatterer but not from each other. In figure 4.1.8 the decrease of the cost functional is depicted and it can be easily observed that it reaches lower values than before, something expected as the reconstruction results are better.

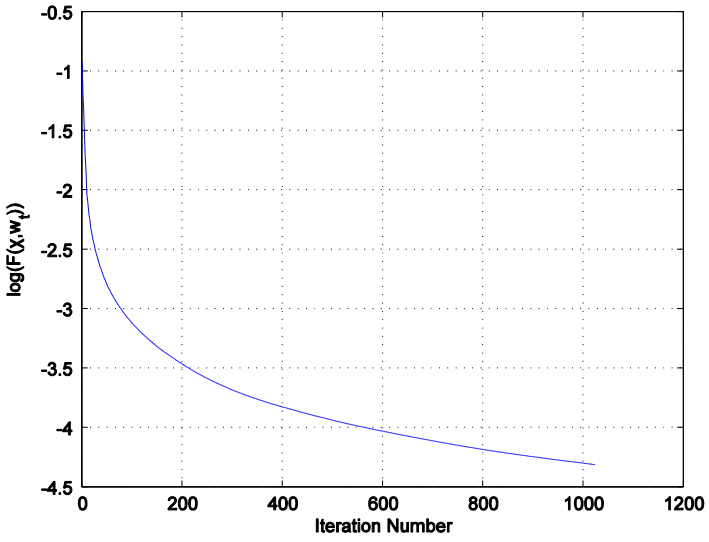

Figure 4.1.8. Cost functional

4.2 E-phantom profile

In order to compare the FEM-CSI and FEM-MRCSI method the scatterer of figure 5.2.1 was selected. The scatterer was placed at a square background medium of $\varepsilon_{r_b} = 1$ with a side of 0.13m. It is illuminated by 24 sources at a frequency $f = 5GHz$ uniformly distributed over a circle of radius 0.174m and measurements are taken by 24 uniformly distributed over a circle of radius of 0.102m. The relative dielectric permeability was $\varepsilon_r = 2.3$, with the nodes inside the imaging domain D amounting to 4044 and in the total domain Ω to 34458.

By comparing the results (fig 4.2.2a 4.2.2b) from the two methods, it can be easily noted that in the case of the FEM-MRCSI the reconstruction results are better since the values of the reconstructed dielectric permittivity are closer to the actual ones with the edges of the scatterer better. Furthermore, it is clear that a smoother reconstruction is performed without extreme values inside the scatterer where the

contrast denotes similar values. Finally the error was 15.38% in case of the FEM-CSI method and 15.04% in case of the FEM-MRCSI method.

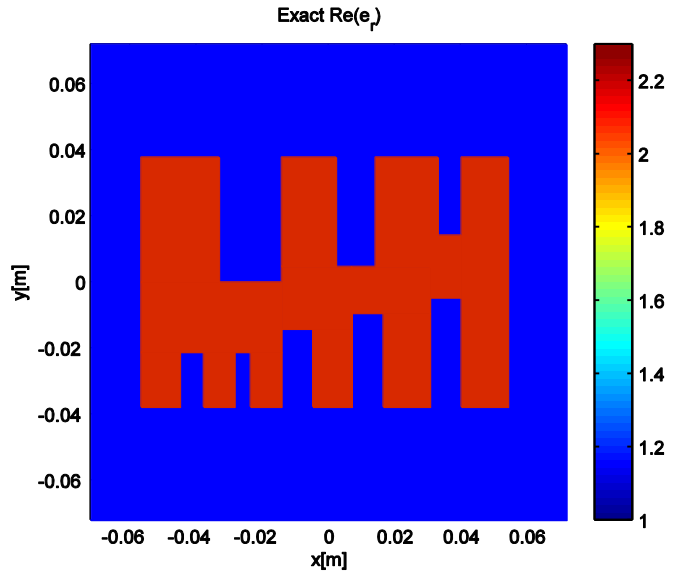

Figure 4.2.1. Real part Re{ε_r} of relative dielectric permeability

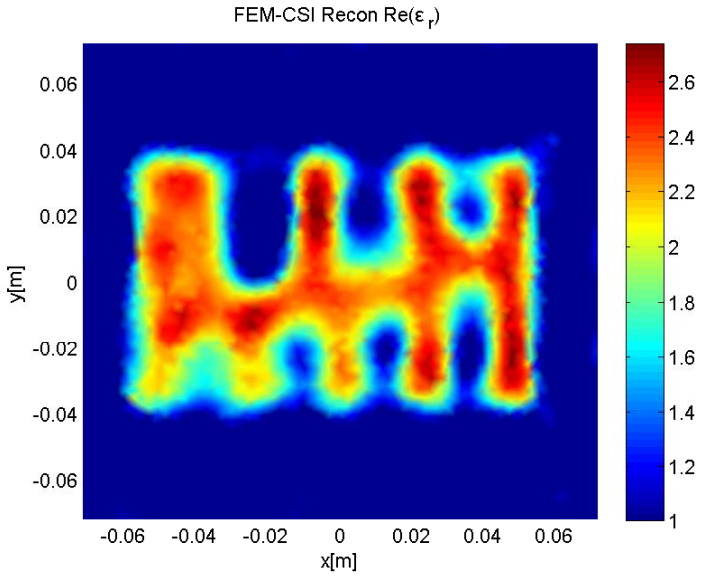

Figure 4.2.2a. Reconstructed relative dielectric permeability with the FEM-CSI method

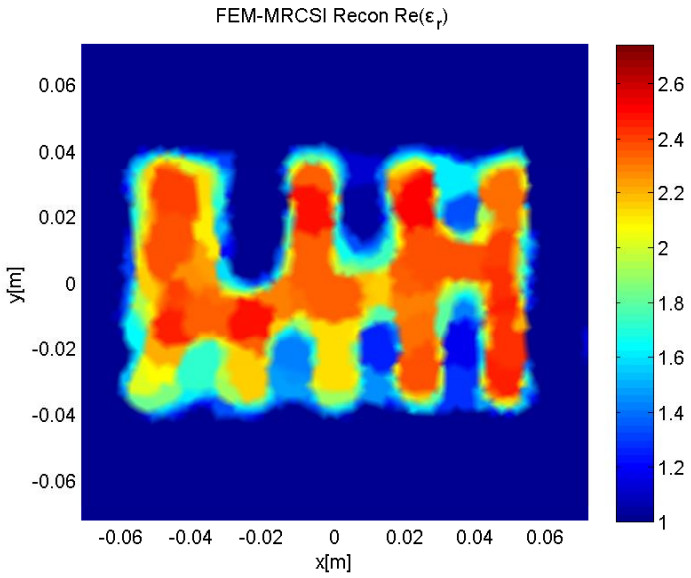

Figure 4.2.2b. Reconstructed relative dielectric permeability with the FEM-MRCSI method

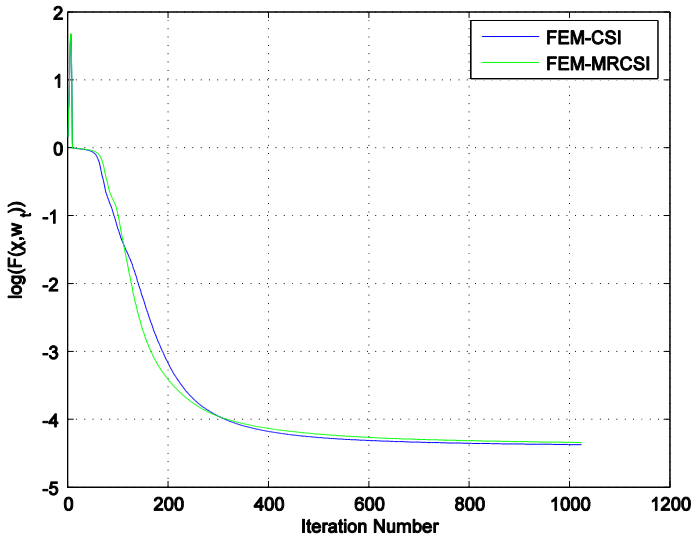

Figure 4.2.3. Cost functional of FEM-CSI and FEM-MRCSI methods

4.3 Concentric squares profile

The last scatterer that was simulated was the one depicted in figures 4.3.1a and 4.3.1b. It comprises of two concentric squares of different relative dielectric permeability. It is illuminated by 30 sources and measurements are taken by 30 receivers. The sources are uniformly distributed on a circle of radius of 1.2m, whereas the receivers are located on a concentric circle of radius of 0.81m. The complex relative dielectric permeability of the outer scatterer is $\varepsilon_r = 1.3 - j0.4$, whereas the inner ones' is $\varepsilon_r = 1.6 - j0.2$ and they are placed on a background medium of $\varepsilon_{r_b} = 1$. The imaging domain D with width of 0.9m comprises of 4569 nodes, whereas the nodes in the total domain Ω amount to 34560.

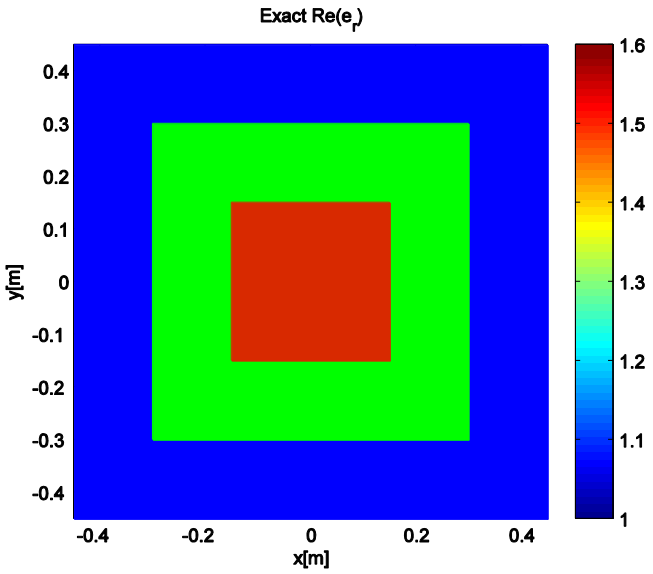

Figure 4.3.1a. Real part Re{e_r} of complex relative permeability

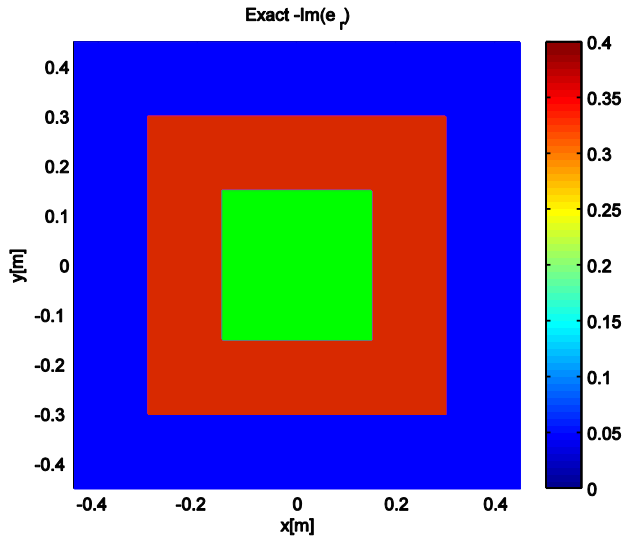

Figure 4.3.1b. Imaginary part -Im{e_r} of complex relative permeability

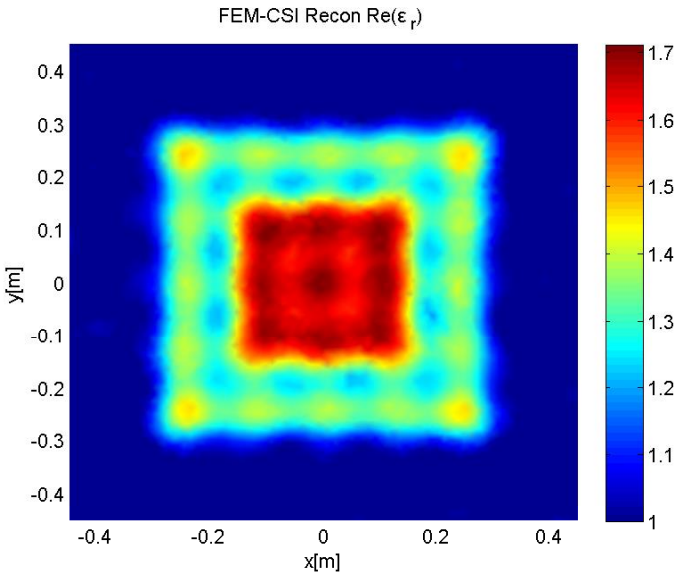

Figure 4.3.2a. Reconstructed real part Re{ε_r} of complex relative dielectric permeability with FEM-CSI method

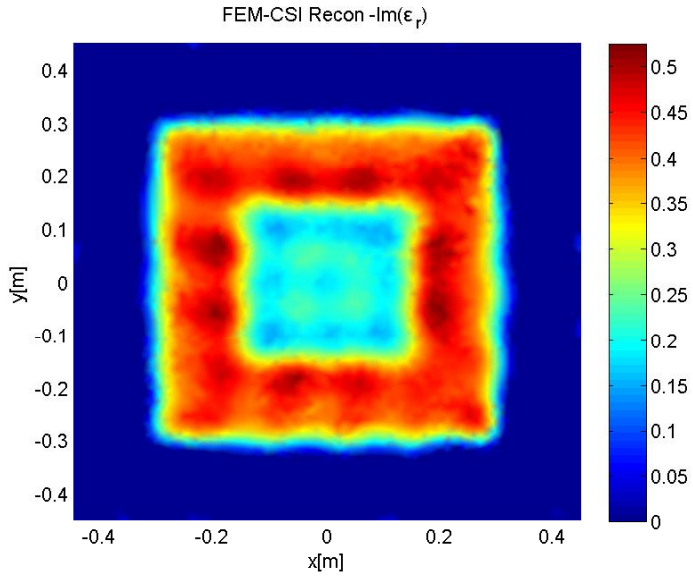

Figure 4.3.2b. Reconstructed imaginary part –Im{ε_r} of complex relative dielectric permeability with FEM-CSI method

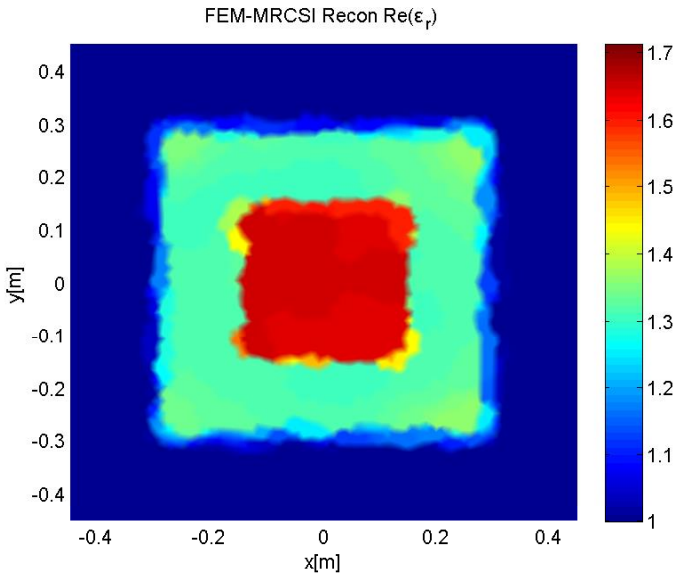

Figure 4.3.3a. Reconstructed real part Re{ε_r} of complex relative dielectric permeability with FEM-MRCSI method

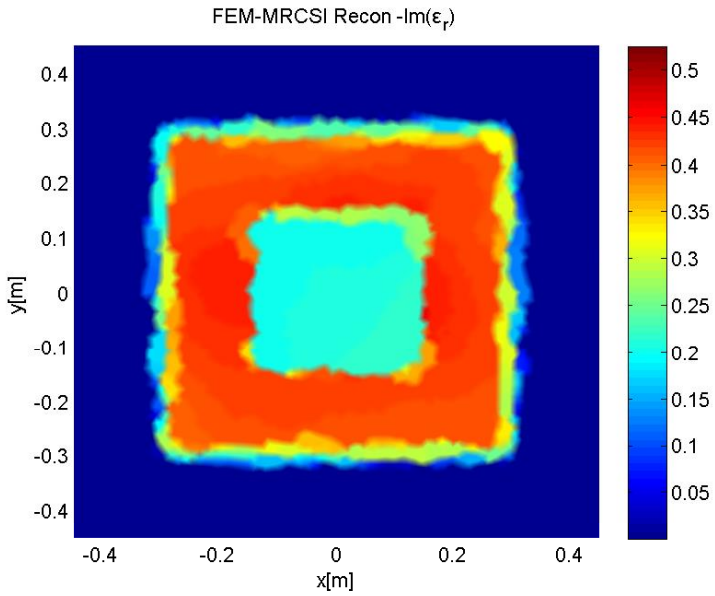

Figure 4.3.3b. Reconstructed imaginary part –Im{ε_r} of complex relative dielectric permeability with FEM-MRCSI method

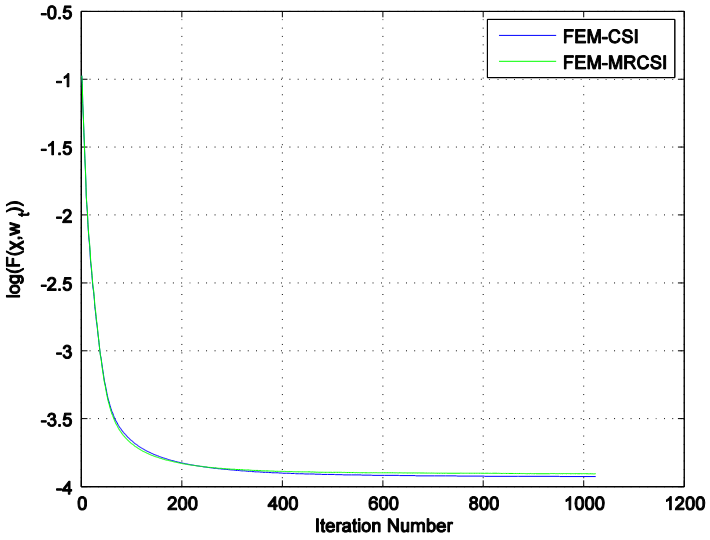

Figure 4.3.4. Cost functional of FEM-CSI methods FEM-MRCSI comparison

By observing the figure results (4.3.2, 4.3.3, 4.3.4) for the concentric squares scatterer we can easily confirm the conclusions derived by the E-phantom scatterer inversion. In the case of the FEM-MRCSI for the concentric squares the reconstructed values approach the actual ones better leading to almost the same contrast values, with the different areas having almost the same reconstructed values without abnormal peaks. Finally the error in case of the FEM-CSI method was 6.1%, whereas in the case of the FEM-MRCSI method was 5.41%

4.4 Definition of contrast to the problem elements suggestion

Both the methods FEM-CSI and FEM-MRCSI define the contrast variable on the problems nodes of the finite elements mesh. This definition incorporates a linearization in the relative dielectric permeability, which has no physical meaning. On the context of the present thesis an attempt to define the contrast variable over the problems triangular elements was made. Since the contrast source incorporates the values of the electric fields it has to be defined over the nodes of the mesh. Hence an operator M_E is suggested which transforms the values of contrast from the mesh nodes to the problem's mesh triangles.

By presuming a matrix operator $\mathbf{M_E} \in \mathbb{R}^{I \times N_E}$, where I is the number of nodes inside the imaging domain D and N_E is the number of elements inside the domain. Surmising a node i as presented in figure 4.4.1, the elements which the node belongs and

A_j the area of the j-th element which the node i belongs. The operator is a sparse matrix since in the i-th row of the matrix non zero are the elements of the j-th rows, hence the rows which have the same index as the numeration of the j-th elements which the node i belongs being equal to $\frac{A_j}{\sum_j A_j}$.

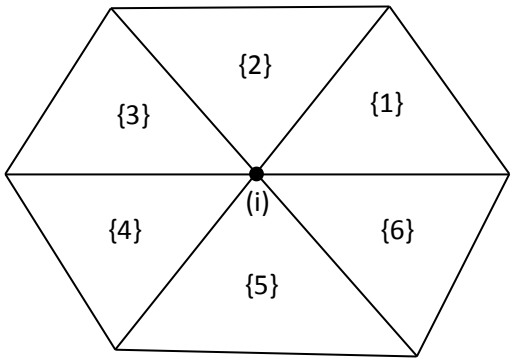

Fgiure 4.4.1. Node i and the elements j=1,2,…,6 where it belongs

The contrast source terms are given by:

$$w_i = \frac{\sum_j \sum_{k=1}^{3} \chi_k^j A_j}{\sum_j A_j} \tag{4.4}$$

The incorporation of the operator M_E varies the calculating equations of the contrast, derivatives and the domain error as:

$$\left(\sum_t \mathbf{M}_E^H \mathbf{E}_{t,n}^H \mathbf{T}_D \mathbf{E}_{t,n} \mathbf{M}_E \right) \chi_n = \sum_t \mathbf{M}_E^H \mathbf{E}_{t,n}^H \mathbf{T}_D w_{t,n} \tag{4.5}$$

$$g_{t,n} = -2\eta_S \mathbf{T}_D^{-1} \mathbf{L}^H \mathbf{M}_S^H \rho_{t,n-1} - 2\eta_{D,n} \mathbf{T}_D^{-1} \left(\mathbf{I} - \mathbf{L}^H \mathbf{M}_D^H \mathbf{Q}_{n-1}^H \right) \mathbf{T}_D r_{t,n-1} \tag{4.6}$$

$$r_{t,n} = \mathbf{M}_E \chi_n \odot E_t^{inc} - w_{t,n} + \mathbf{M}_E \chi_n \odot \mathbf{M}_D \mathbf{L} \left[w_{t,n} \right] \tag{4.7}$$

where $\mathbf{Q}$ is a diagonal matrix with elements $\mathbf{Q} = diag\left(\mathbf{M}_E \chi_n \right)$.

After several tests in different scatterers and meshes, in all cases equation (4.5) lead to over defined system of equations since the rank of the of the matrix in the left hand side of the equation was always equal to the number of nodes inside the imaging domain D. A solution to this problem would be to try to solve the system with a pseudo inverse approach. If equation (4.5) is written as $\mathbf{A}\chi_n = \mathbf{B}$ then the aforementioned approach will lead to

$$\mathbf{A}\chi_n = \mathbf{B} \Leftrightarrow$$
$$\mathbf{A}^H\mathbf{A}\chi_n = \mathbf{A}^H\mathbf{B} \Leftrightarrow$$
$$\chi_n = \left(\mathbf{A}^H\mathbf{A}\right)^{-1}\mathbf{A}^H\mathbf{B} \Leftrightarrow$$

$$\chi_n = \mathbf{A}^{+}\mathbf{B} \tag{4.8}$$

Such an approach leads to a dense system of equations, which requires even greater computational resources, thus suppressing the advantage of the FEM methods the creation of a sparse system of equations. The fact that the system's rank was always equal to the number of nodes leads to the assumption that all the information is stored to the problem's nodes. Several other thoughts were made but none of them led to a resulting possible definition of the contrast variables in the meshes' finite elements. Hence this dual scheme of defining the contrast and the contrast source in different ways although being a reasonable approach does not seem to be able to model the inversion problem.

5. CONCLUSIONS - FURTHER WORK SUGGESTIONS

In the present dissertation a generalized code was implemented for modeling FEM-CSI and FEM-MRCSI. The code was implemented in MATLAB and attempts were made to be as vectorized as possible and it allows the incorporation of any 2-D geometry. It is clear from the derived results that both mentioned techniques are capable of providing very promising inversion results. They also have the ability of modeling inhomogeneous background mediums of an arbitrary shape. It is also clear that the FEM-MRCSI method lead to smoother reconstructions since it seems to have the ability of "sensing" the different areas and annotating almost equal contrast values to them. In some publications [9,14, 20, 21, 22] as step update for the contrast source variables is considered only the real part of the derived coefficient. A similar approach was tested in the current thesis but lead to no significant differences in the resulting reconstructed profiles. A drawback that can be mentioned is the extremely high operation time for a full run of the algorithm around 58 hours. As of today no known theoretical limit for the resolution of the inversion techniques has been proposed. It has been suggested [5] that the ability to separate scatterers is affected by the SNR of the implementation and not the wavelength. Furthermore, it has been proposed [5] that measuring evanescent vector fields lead to increased resolution. There are of course further fields that can be researched further.

The PML boundary conditions are mandatory when open spaces are simulated. The complex parameters of the PML however affect the convergence of the algorithm that calculates the scattered fields as well as the convergence of the inversion algorithms. It is not clear how these ramifications on the convergence affect the resolution of the inversion technique. Absorbing boundary conditions can be incorporated in the aforementioned methods in order to detect any improvements in the resolution.

Another possible improvement could be the use of higher order triangular elements or the refinement of the mesh in areas where there is a possibility that a scatterer exists. The first approach does not increase much the complexity of the problem, while the second does, but leads to certain other mathematical problems [1]. In the second approach a technique to select areas of refinement would be to set a threshold over which the calculated derivative would leads us to select the areas to be refined, since derivative with high values indicate the potential existence of a scatterer.

A multifrequency approach can lead to better reconstructions [9, 28, 29, 30, 31,32]. In such an approach either the data from different frequencies are used simultaneously or the reconstructed result of a certain frequency is given as an initial guess for the inversion algorithm at the next frequency.

In the present thesis TM excitation waves were used. However, as it has already been mentioned the use of TE waves is also possible. From a physical point of view, the two polarizations are independent form one another and each one carries different information. Thus a simultaneous inversion of both polarizations is possible to lead to better reconstructions.

As already mentioned in chapter 4 the definition of the contrast in the nodes of the problem does not seem to have a direct physical meaning due to the resulting linearization. The solutions to declutch the contrast from the nodes did not lead to any results. The definition of the contrast in the problems elements is a field of study that can lead to an approach to the problem without the unwanted linearization derived from the base functions of the finite element technique.

Finally due to the high simulation runtimes it is reasonable to implement the algorithm using parallel computing for its execution in GPU processors or clusters thus making the examination of 3-D geometries with the development of vector finite element implementations .

APPENDIX A

MATHEMATICAL FORMULATION OF EQUATIONS TO CALCULATIN SCATTERING USING FEM

In the scattering problem the Maxwell equations apply

$$\vec{\boldsymbol{E}}_{tot} = \vec{\boldsymbol{E}}_i + \vec{\boldsymbol{E}}_s \tag{A.1}$$

$$\nabla \times \vec{\mathbf{E}}_{tot} = -j\omega \bar{\mu}_r \mu_0 \vec{\mathbf{H}}_{tot} \tag{A.2}$$

$$\nabla \times \vec{\mathbf{H}}_{tot} = -j\omega \bar{\varepsilon}_r \varepsilon_0 \vec{\mathbf{E}}_{tot} \tag{A.3}$$

By starting form equations (A.2) we try to end up in (2.19)

$$\begin{aligned}
&\nabla \times \vec{\mathbf{E}}_{tot} = -j\omega \bar{\mu}_r \mu_0 \vec{\mathbf{H}}_{tot} \Leftrightarrow \\
&\bar{\mu}_r^{-1} \nabla \times \vec{\mathbf{E}}_{tot} = -j\omega \mu_0 \vec{\mathbf{H}}_{tot} \Leftrightarrow \\
&\nabla \times \left(\bar{\mu}_r^{-1} \nabla \times \vec{\mathbf{E}}_{tot} \right) = -j\omega \mu_0 \nabla \times \vec{\mathbf{H}}_{tot} \Leftrightarrow \\
&\nabla \times \bar{\mu}_r^{-1} \nabla \times \vec{\mathbf{E}}_{tot} = \omega^2 \varepsilon_0 \mu_0 \bar{\varepsilon}_r \vec{\mathbf{E}}_{tot} \Leftrightarrow \\
&\nabla \times \bar{\mu}_r^{-1} \nabla \times \vec{\mathbf{E}}_{tot} - k_0^2 \bar{\varepsilon}_r \vec{\mathbf{E}}_{tot} = 0 \Leftrightarrow
\end{aligned}$$

$$\nabla \times \bar{\mu}_r^{-1} \nabla \times \vec{\mathbf{E}}_S - k_0^2 \bar{\varepsilon}_r \vec{\mathbf{E}}_S = -\nabla \times \bar{\mu}_r^{-1} \nabla \times \vec{\mathbf{E}}_i + k_0^2 \bar{\varepsilon}_r \vec{\mathbf{E}}_i \tag{A.4}$$

In free space the following equation applies:

$$\nabla \times \nabla \times \vec{\mathbf{E}}_i - k_0^2 \vec{\mathbf{E}}_i = 0 \tag{A.5}$$

Combining equations (A.4) and (A.5)

$$\nabla \times \bar{\mu}_r^{-1} \nabla \times \vec{\mathbf{E}}_S - k_0^2 \bar{\varepsilon}_r \vec{\mathbf{E}}_S = -\nabla \times \bar{\mu}_r^{-1} \nabla \times \vec{\mathbf{E}}_i + k_0^2 \bar{\varepsilon}_r \vec{\mathbf{E}}_i + \nabla \times \nabla \times \vec{\mathbf{E}}_i - k_0^2 \vec{\mathbf{E}}_i \Leftrightarrow$$

$$\nabla \times \bar{\mu}_r^{-1} \nabla \times \vec{\mathbf{E}} - k_0^2 \bar{\varepsilon}_r \vec{\mathbf{E}} = -\nabla \times \left(\bar{\mu}_r^{-1} - \bar{1} \right) \nabla \times \vec{\mathbf{E}}_i + k_0^2 \left(\bar{\varepsilon}_r - \bar{1} \right) \vec{\mathbf{E}}_i \tag{A.6}$$

It is desirable to specify the exact elements of the FEM matrix equations. As already mentioned in chapter 2 the Galerkin formulation for calculating scattering is

$$\begin{aligned}\iint_S \vec{\mathbf{E}}' \cdot \left(\nabla \times \bar{\mu}_r^{-1} \nabla \times \vec{\mathbf{E}}\right) ds - \iint_S \vec{\mathbf{E}}' \cdot k_0^2 \bar{\varepsilon}_r \vec{\mathbf{E}} ds = \\ - \iint_S \vec{\mathbf{E}}' \cdot \left(\nabla \times \left(\bar{\mu}_r^{-1} - 1\right) \nabla \times \vec{\mathbf{E}}_i\right) ds + \iint_S \vec{\mathbf{E}}' \cdot k_0^2 \left(\bar{\varepsilon}_r - 1\right) \vec{\mathbf{E}}_i ds\end{aligned} \tag{A.7}$$

The first integral in the left hand side of the above equation with the us the vector identity $\nabla \cdot (\mathbf{A} \times \mathbf{B}) = \mathbf{B} \cdot \nabla \times \mathbf{A} - \mathbf{A} \cdot \nabla \times \mathbf{B}$ is

$$\iint_S \vec{\mathbf{E}}' \cdot \left(\nabla \times \bar{\mu}_r^{-1} \nabla \times \vec{\mathbf{E}}\right) ds = \iint_S \nabla \cdot \left(\bar{\mu}_r^{-1} \nabla \times \vec{\mathbf{E}} \times \vec{\mathbf{E}}'\right) ds + \iint_S \nabla \times \vec{\mathbf{E}}' \cdot \bar{\mu}_r^{-1} \nabla \times \vec{\mathbf{E}} ds$$

With the help of the Gauss theorem the above equation is

$$\begin{aligned}\iint_S \vec{\mathbf{E}}' \cdot \left(\nabla \times \bar{\mu}^{-1} \nabla \times \vec{\mathbf{E}}\right) ds &= \oint_{\partial S} \left(\bar{\mu}^{-1} \nabla \times \vec{\mathbf{E}} \times \vec{\mathbf{E}}'\right) \hat{n} \cdot dl + \iint_S \nabla \times \vec{\mathbf{E}}' \cdot \bar{\mu}^{-1} \nabla \times \vec{\mathbf{E}} ds \\ &= -\oint_{\partial S} \left(\vec{\mathbf{E}}' \times \bar{\mu}^{-1} \nabla \times \vec{\mathbf{E}}\right) \hat{n} \cdot dl + \iint_S \nabla \times \vec{\mathbf{E}}' \cdot \bar{\mu}^{-1} \nabla \times \vec{\mathbf{E}} ds \\ &= -\oint_{\partial S} \vec{\mathbf{E}}' \cdot \left(\bar{\mu}^{-1} \nabla \times \vec{\mathbf{E}} \times \hat{n}\right) \cdot dl + \iint_S \nabla \times \vec{\mathbf{E}}' \cdot \bar{\mu}^{-1} \nabla \times \vec{\mathbf{E}} ds\end{aligned}$$

The cross product of the line integral of the above relation is either a vector pointing at x or at y, hence inner multiplied with $\vec{\mathbf{E}}'$ leads to zero. Thus we the following equation is derived:

$$\iint_S \vec{\mathbf{E}}' \cdot \left(\nabla \times \bar{\mu}_r^{-1} \nabla \times \vec{\mathbf{E}}\right) ds = \iint_S \nabla \times \vec{\mathbf{E}}' \cdot \bar{\mu}_r^{-1} \nabla \times \vec{\mathbf{E}} ds \tag{A.8}$$

In a similar way the first integral of the right hand side of equation (A.7) is calculated leading to the relation:

$$\iint_S \vec{\mathbf{E}}' \cdot \left(\nabla \times \left(\bar{\mu}_r^{-1} - 1\right) \nabla \times \vec{\mathbf{E}}\right) ds = \iint_S \nabla \times \vec{\mathbf{E}}' \cdot \left(\bar{\mu}_r^{-1} - 1\right) \nabla \times \vec{\mathbf{E}} ds \tag{A.9}$$

By incorporating the base functions inside the element Ω_n of area A_n of the triangular finite elements mesh into equation (A.7) we have

$$\nabla \times \mathbf{E} = \nabla \times \sum_{j=1}^{3} E_j \mathbf{N}_j = \frac{\partial E_z}{\partial y} \hat{x} - \frac{\partial E_z}{\partial x} \hat{y} \tag{A.10}$$

With the help of equation (A.10) equation (A.7) is

$$\begin{aligned}\iint_{\Omega_n} \vec{\mathbf{E}}' \cdot \left(\nabla \times \bar{\mu}_r^{-1} \nabla \times \vec{\mathbf{E}}\right) ds &= \sum_{i=1}^{3}\sum_{j=1}^{3} E_i' \iint_{\Omega_n} \left(\frac{\partial N_i}{\partial y} \mu_{r_x}^{-1} \frac{\partial N_j}{\partial y} + \frac{\partial N_i}{\partial x} \mu_{r_y}^{-1} \frac{\partial N_j}{\partial x} \right) ds E_j \\ &= \sum_{i=1}^{3}\sum_{j=1}^{3} E_i' S_{ij} E_j\end{aligned} \tag{A.11}$$

where

$$S_{ij} = \left(c_i \mu_{r_x}^{-1} c_j + b_i \mu_{r_y}^{-1} b_j \right) A_n \tag{A.11}$$

In a similar way the rest of the integrals can be calculated.

The first integral of the right hand side of (A.7) is

$$\iint_{\Omega_n} \vec{\mathbf{E}}' \cdot \left(\nabla \times \left(\bar{\mu}_r^{-1} - 1 \right) \nabla \times \vec{\mathbf{E}}\right) ds = \sum_{i=1}^{3}\sum_{j=1}^{3} E_i' S_{ij}'' E_j \tag{A.12}$$

$$S_{ij}'' = \left[c_i \left(\mu_{r_x}^{-1} - 1 \right) c_j + b_i \left(\mu_{r_y}^{-1} - 1 \right) b_j \right] A_n \tag{A.13}$$

The second integral of the left hand side of (A.7) is

$$\iint_{S} \vec{\mathbf{E}}' \cdot k_0^2 \bar{\varepsilon}_r \vec{\mathbf{E}} ds = k_0^2 \sum_{i=1}^{3}\sum_{j=1}^{3} E_i' T_{ij} E_j \tag{A.14}$$

$$T_{ij} = \varepsilon_{r_z} \iint_{\Omega_n} \zeta_i \zeta_j ds \tag{A.15}$$

The second integral of the right hand side of (A.7) is

$$\iint_{S} \vec{\mathbf{E}}' \cdot k_0^2 \left(\bar{\varepsilon}_r - 1 \right) \vec{\mathbf{E}} ds = k_0^2 \sum_{i=1}^{3}\sum_{j=1}^{3} E_i' T_{ij}'' E_j \tag{A.16}$$

$$T_{ij}'' = \left(\varepsilon_{r_z} - 1 \right) \iint_{\Omega_n} \zeta_i \zeta_j ds \tag{A.17}$$

APPENDIX B

MATHEMATICAL FORMULATION OF FEM-CSI EQUATIONS

B.1 Derivative calculation of the cost functional of the FEM-CSI method

In the first step of the FEM-CSI method it is imperative to calculate the derivatives $g_{t,n}$ of the cost functional corresponding to the contrast sources. In a point w_t, g_t is a vector pointing to the direction were the Gâteaux derivative is maximized.

The Gâteaux derivative is calculated first for the data equation $F^S(w_t)$ and then for the domain equation $F^D(\chi, w_t)$. For a small variation of w_t over a direction h_t, the Gâteaux derivative for the data equation $F^S(w_t)$ is given by:

$$
\begin{aligned}
d_{h_t} F^S(w_t) &= \lim_{\varepsilon\to 0} \frac{F^S(w_t) + F^S(w_t + \varepsilon h_t)}{\varepsilon} \\
&= \lim_{\varepsilon\to 0} \eta_S \frac{\left\| \tilde{E}_t^S - \mathbf{M}_S \mathbf{L}[w_t + \varepsilon h_t] \right\|_S^2 - \left\| \tilde{E}_t^S - \mathbf{M}_S \mathbf{L}[w_t] \right\|_S^2}{\varepsilon} \\
&= \lim_{\varepsilon\to 0} \eta_S \frac{\left\| \rho_t - \varepsilon \mathbf{M}_S \mathbf{L}[h_t] \right\|_S^2 - \left\| \rho_t \right\|_S^2}{\varepsilon} \\
&= \lim_{\varepsilon\to 0} \eta_S \frac{\left\| \rho_t \right\|_S^2 - 2\varepsilon \operatorname{Re}\left\langle \mathbf{M}_S \mathbf{L}[h_t], \rho_t \right\rangle_S + \varepsilon^2 \left\| \mathbf{M}_S \mathbf{L}[h_t] \right\|_S^2 - \left\| \rho_t \right\|_S^2}{\varepsilon} \\
&= \lim_{\varepsilon\to 0} \eta_S \frac{-2\varepsilon \operatorname{Re}\left\langle \mathbf{M}_S \mathbf{L}[h_t], \rho_t \right\rangle_S + \varepsilon^2 \left\| \mathbf{M}_S \mathbf{L}[h_t] \right\|_S^2}{\varepsilon} \\
&= \operatorname{Re}\left\langle -2\eta_S \mathbf{M}_S \mathbf{L}[h_t], \rho_t \right\rangle_S
\end{aligned}
\tag{B.1}
$$

For the calculation of h_t, the direction i.e. that maximizes the derivative we can define a conjugate operator $\mathbf{G}^S$ which satisfies the equation

$$
\left\langle -2\eta_S \mathbf{M}_S \mathbf{L}[h_t], \rho_t \right\rangle_S = \left\langle h_t, \mathbf{G}^S[\rho_t] \right\rangle_D \tag{B.2}
$$

By using the definition of the inner product that was given in equations (3.33) and (3.36) equation (B.2) is

$$-2\eta_S \rho_t^H \mathbf{M}_S \mathbf{L}\left[h_t\right] = \rho_t^H \left(\mathbf{G}^S\right)^H \mathbf{T}_D h_t \tag{B.3}$$

It can be proven rather easily that $\mathbf{G}^S = -2\eta_S \mathbf{T}_D^{-1} \mathbf{L}^H \mathbf{M}_S^H$ with the Gâteaux derivative being transformed as

$$d_{h_t} F^S\left(w_t\right) = \mathrm{Re}\left\langle h_t, -2\eta_S \mathbf{T}_D^{-1} \mathbf{L}^H \mathbf{M}_S^H \left[\rho_t\right]\right\rangle_S \tag{B.4}$$

To maximize the derivative, direction h_t is selected as

$$h_t = -2\eta_S \mathbf{T}_D^{-1} \mathbf{L}^H \mathbf{M}_S^H \left[\rho_t\right] \tag{B.5}$$

Consequently the Gâteaux derivative for the domain equation $F^D\left(\chi, w_t\right)$ must be defined. For a small variation of w_t over a direction h_t the derivative, assuming that the values of χ are constant, is given by the equation:

$$\begin{aligned} d_{h_t} F^D\left(w_t\right) &= \lim_{\varepsilon \to 0} \frac{F^D\left(\chi, w_t + \varepsilon h_t\right) + F^D\left(\chi, w_t\right)}{\varepsilon} \\ &= \lim_{\varepsilon \to 0} \eta_D \frac{\left\| r_t - \varepsilon\left(h_t - \chi \odot \mathbf{M}_D \mathbf{L}\left[h_t\right]\right)\right\|_D^2 - \left\| r_t \right\|_D^2}{\varepsilon} \\ &= \lim_{\varepsilon \to 0} \eta_D \frac{-2\varepsilon\, \mathrm{Re}\left\langle h_t - \chi \odot \mathbf{M}_D \mathbf{L}\left[h_t\right], r_t\right\rangle_D + \varepsilon^2 \left\| h_t - \chi \odot \mathbf{M}_D \mathbf{L}\left[h_t\right]\right\|}{\varepsilon} \\ &= -2\eta_D\, \mathrm{Re}\left\langle h_t - \chi \odot \mathbf{M}_D \mathbf{L}\left[h_t\right], r_t\right\rangle_D \end{aligned} \tag{B.6}$$

In order to calculate the direction h_t equation (B.6) is transformed so that the direction can be isolated. This is done by using the conjugate operator $\mathbf{G}^D$ which satisfies the relation:

$$-2\eta_D \left\langle h_t - \chi \odot \mathbf{M}_D \mathbf{L}\left[h_t\right], r_t\right\rangle_D = \left\langle h_t, \mathbf{G}^D\left[r_t\right]\right\rangle \tag{B.7}$$

With the help of equation (3.33) and the development of the inner product the following equation is denoted

$$-2\eta_D r_t^H \mathbf{T}_D \left(\mathbf{I} - \mathbf{X}\mathbf{M}_D \mathbf{L}\right)\left\langle h_t - \chi \odot \mathbf{M}_D \mathbf{L}\left[h_t\right], r_t\right\rangle_D = \left\langle h_t, \mathbf{G}^D\left[r_t\right]\right\rangle_D \tag{B.8}$$

where $\mathbf{I} \in \mathbb{R}^{I \times I}$ is the identity matrix and $\mathbf{X}_{n-1} = diag\left(\chi_{n-1}\right)$ a diagonal matrix with the values of the contrast. Thus the operator $\mathbf{G}^D$ is given by equation:

$$\mathbf{G}^D = -2\eta_D \mathbf{T}_D^{-1}\left(\mathbf{I} - \mathbf{L}^H \mathbf{M}_D^H \mathbf{X}^H\right)\mathbf{T}_D \tag{B.9}$$

The Gâteaux derivative for the domain equation $F^D(\chi, w_t)$ results in

$$d_{h_t} = \left\langle h_t, -2\eta_D \mathbf{T}_D^{-1}\left(\mathbf{I} - \mathbf{L}^H \mathbf{M}_D^H \mathbf{X}^H\right)\mathbf{T}_D r_t \right\rangle_D \tag{B.10}$$

with the direction h_t which maximizes (B.10) to be equal with

$$h_t = -2\eta_D \mathbf{T}_D^{-1}\left(\mathbf{I} - \mathbf{L}^H \mathbf{M}_D^H \mathbf{X}^H\right)\mathbf{T}_D r_t \tag{B.11}$$

The derivative of the cost functional corresponding to the n-th iteration of the algorithm is for the contrast source $w_{t,n-1}$ and contrast χ_{n-1}

$$g_{t,n} = -2\eta_S \mathbf{T}_D^{-1} \mathbf{L}^H \mathbf{M}_S^H \left[\rho_{t,n-1}\right] - 2\eta_D \mathbf{T}_D^{-1}\left(\mathbf{I} - \mathbf{L}^H \mathbf{M}_D^H \mathbf{X}^H\right)\mathbf{T}_D r_{t,n-1} \tag{B.12}$$

B.2 Contrast calculation

In a second step of the FEM-CSI method, after having calculated the values of the contrast source, the values of the contrast χ which minimize the domain equation are calculated

$$F^D(\chi, w_t) = \left\| \mathbf{E}_t \chi - w_t \right\|_D^2 \tag{B.13}$$

where $\mathbf{E}_t$ is a diagonal matrix whose elements are the total field values, which are given by relation $\mathrm{E}_t = E_t^{inc} + \mathbf{M}_D \mathbf{L}\left[w_t\right]$. In this step the values of the contrast source are considered as constants.

The minimizer of equation (B.13) is given again with the help of the Gâteaux derivatives. As before, for a small variation of the contrast χ over a direction h the derivative is calculated as:

$$\begin{aligned} dhF^D(\chi) &= \lim_{\varepsilon \to 0} \frac{1}{\varepsilon}\left[\sum_t \left\| \mathbf{E}_t\left(\chi + \varepsilon h\right) - w_t \right\|_D^2 - \sum_t \left\| \mathbf{E}_t \chi - w_t \right\|_D^2 \right] \\ &= \lim_{\varepsilon \to 0} \frac{1}{\varepsilon}\left[\sum_t \left\| \left(\mathbf{E}_t \chi - w_t\right) + \varepsilon \mathbf{E}_t h \right\|_D^2 - \sum_t \left\| \mathbf{E}_t \chi - w_t \right\|_D^2 \right] \\ &= \lim_{\varepsilon \to 0} \frac{1}{\varepsilon}\left[\sum_t \left\| r_t + \varepsilon \mathbf{E} h \right\|_D^2 - \sum_t \left\| r_t \right\|_D^2 \right] \end{aligned}$$

$$= \lim_{\varepsilon \to 0} \frac{1}{\varepsilon} \left[\sum_t \left\| r_t \right\|_D^2 + 2\varepsilon \sum_t \mathrm{Re} \left\langle r_t, \mathbf{E}_t h \right\rangle_D + \varepsilon^2 \sum_t \left\| \mathbf{E}_t h \right\| - \sum_t \left\| r_t \right\|_D^2 \right]$$

$$= 2 \sum_t \mathrm{Re} \left\langle r_t, \mathbf{E}_t h \right\rangle_D$$

$$= 2 \sum_t \mathrm{Re} \left(h^H \mathbf{E}_t^H \mathbf{T}_D r_t \right)$$

$$= 2 \,\mathrm{Re} \left\langle \sum_t \mathbf{E}_t^H \mathbf{T}_D r_t, h \right\rangle \tag{B.14}$$

The operator $\langle\ \rangle$ corresponds to the inner product of two vectors in a n-dimensional space which for a two random vectors α, b is defined as $\langle a, b \rangle = b^H a$. The direction which maximizes the equation (B.14) can be easily computed as $h = \sum_t \mathbf{E}_t^H \mathbf{T}_D r_t$. Hence in the n-th iteration of the FEM-CSI algorithm the derivative of the domain equation corresponding to the contrast χ_n is

$$\nabla F^D(\chi)\big|_{\chi=\chi_n} = \sum_t \mathbf{E}_{t,n}^H \mathbf{T}_D \left(\mathbf{E}_{t,n} \chi_n - w_{t,n} \right) \tag{B.15}$$

The values of contrast χ_n which minimize equation (B.13) are calculated by setting the equation (B.15) equal to zero.

$$\left(\sum_t \mathbf{E}_{t,n}^H \mathbf{T}_D \mathbf{E}_{t,n} \right) \chi_n = \sum_t \mathbf{E}_{t,n}^H \mathbf{T}_D w_{t,n} \tag{B.16}$$

B.3 Initialization of the FEM-CSI method

An initial estimation is necessary for the initialization of the FEM-CSI algorithm which is calculated by minimizing the following relation over the steepest-descent direction

$$F^S(w_t) = \left\| \tilde{\mathrm{E}}_t^S - \mathbf{M}_S \mathbf{L} [w_t] \right\|_S^2 \tag{B.17}$$

As it has already be proven in appendix A in the n-th iteration of the algorithm the derivative of equation (B.17) corresponding to $w_{t,n-1}$ is given by the relation:

$$\nabla F^S(w_t)\big|_{w_t = w_{t,n-1}} = -2\eta_S \mathbf{T}_D^{-1} \mathbf{L}^H \mathbf{M}_S^H \left[\rho_{t,n-1} \right] = \mathbf{G}^S \rho_{t,n-1} \tag{B.18}$$

The update for the first iteration with the steepest descent method is

$$w_{t,0} = w_{t,-1} - \beta_0 \mathbf{G}^S \rho_{t,-1} \tag{B.19}$$

where the value $w_{t,-1}$ is set to zero corresponding to the initial guess of the steepest-descent method. As β_0 we define the actual value that minimizes $F^S\left(w_{t,-1} - \beta_0 \mathbf{G}^S \rho_{t,-1}\right)$ and be calculated as:

$$\begin{aligned} F^S\left(w_{t,0}\right) &= \left\| \tilde{E}_t^S + \beta_0 \mathbf{M}_S \mathbf{L}\left[\mathbf{G}^S \tilde{E}_t^S\right] \right\|_S^2 \\ &= \left(\tilde{E}_t^S + \beta_0 \mathbf{M}_S \mathbf{L}\left[\mathbf{G}^S \tilde{E}_t^S\right]\right)^H \left(\tilde{E}_t^S + \beta_0 \mathbf{M}_S \mathbf{L}\left[\mathbf{G}^S \tilde{E}_t^S\right]\right) \\ &= \left\| \tilde{E}_t^S \right\|_S^2 + 2\beta_0 \,\mathrm{Re}\left\langle \mathbf{M}_S \mathbf{L}\left[\mathbf{G}^S \tilde{E}_t^S\right], \tilde{E}_t^S \right\rangle_S + \beta_0^2 \left\| \mathbf{M}_S \mathbf{L}\left[\mathbf{G}^S \tilde{E}_t^S\right] \right\|_S^2 \end{aligned} \tag{B.20}$$

Differentiating equation (B.20) corresponding to β_0 and setting the derivative equal to zero we denote to the equation:

$$\beta_0 = -\frac{\mathrm{Re}\left\langle \mathbf{M}_S \mathbf{L}\left[\mathbf{G}^S \tilde{E}_t^S\right], \tilde{E}_t^S \right\rangle_S}{\left\| \mathbf{M}_S \mathbf{L}\left[\mathbf{G}^S \tilde{E}_t^S\right] \right\|_S^2} \tag{B.21}$$

Incorporating equation (B.21) into equation (B.19) the initial step of the FEM-CSI method has been fully derived and is given by the equation:

$$w_{t,0} = \frac{\mathrm{Re}\left\langle \mathbf{M}_S \mathbf{L}\left[\mathbf{G}^S \tilde{E}_t^S\right], \tilde{E}_t^S \right\rangle_S}{\left\| \mathbf{M}_S \mathbf{L}\left[\mathbf{G}^S \tilde{E}_t^S\right] \right\|_S^2} \mathbf{G}^S \tilde{E}_t^S \tag{B.22}$$

APPENDIX C

MATHEMATICAL FORMULATION OF FEM-MRCSI EQUATIONS

C.1 Calculating the derivatives of the FEM-MRCSI method cost functional

In the FEM-MRCSI method it is essential to calculate the derivative of the cost functional corresponding to contrast χ. The definition of the derivatives of the term $F^{CSI}(\chi, w_t)$ has already been explained in appendix B.2. For the $F^{MR}(\chi)$, working again with the use of the Gâteaux derivatives the derivation of the derivatives is

$$\begin{aligned} d_h F_n^{MR}(\chi) &= \lim_{\varepsilon\to 0} \frac{F_n^{MR}(\chi+\varepsilon h) - F_n^{MR}(\chi)}{\varepsilon} \\ &= \lim_{\varepsilon\to 0} \frac{\left\|b_n \nabla(\chi+\varepsilon h)\right\|_D^2 - \left\|b_n \nabla \chi\right\|_D^2}{\varepsilon} \\ &= \lim_{\varepsilon\to 0} \frac{\left\|b_n \nabla \chi\right\|_D^2 + 2\varepsilon \,\mathrm{Re}\left\langle b_n \nabla \chi, b_n \nabla h\right\rangle_D + \varepsilon^2 \left\|b_n \nabla h\right\|_D^2 - \left\|b_n \nabla \chi\right\|_D^2}{\varepsilon} \\ &= 2\,\mathrm{Re}\left\langle b_n \nabla \chi, b_n \nabla h\right\rangle_D \end{aligned} \tag{C.1}$$

Using the vector calculus identity $b\nabla\cdot(\nabla a) = \nabla a\cdot\nabla b + \nabla\cdot(b\nabla a)$ and the divergence theorem equation (C.1) is transformed as:

$$\begin{aligned} \left\langle b_n \nabla \chi, b_n \nabla h\right\rangle_D &= \int_D (b_n \nabla \chi)\overline{(b_n \nabla h)} dv \\ &= \int_D b_n^2 \nabla \chi \overline{\nabla h} dv \\ &= -\int_D \bar{h} \nabla \cdot b_n^2 \nabla \chi dv + \int_D \nabla \cdot \left(b_n^2 \bar{h} \nabla \chi\right) dv \\ &= -\int_D \bar{h} \nabla \cdot b_n^2 \nabla \chi dv + \oint_\Gamma b_n^2 \bar{h} (\nabla \chi \cdot \hat{n}) ds \end{aligned}$$

with the operator $\bar{a}$ deriving the complex conjugate. The line integral of the above equation with the assumption of zero contrast on the boundary Γ of the imaging domain D can be neglected. Thus the following equation can be derived:

$$d_h F_n^{MR}(\chi) = \left\langle -2\nabla \cdot b_n^2 \nabla \chi, h \right\rangle_D \tag{C.2}$$

It can be easily computed that the direction that maximizes the Gâteaux derivative is equal with

$$h = -2\nabla \cdot b_n^2 \nabla \chi \tag{C.3}$$

Hence the derivative of the cost functional corresponding to contrast χ calculated at $\chi = \chi_n^{CSI}$ is given by the equation:

$$g_n^{\chi} = \frac{-2F^{CSI}\left(\chi_n^{CSI}, w_{t,n}\right)\nabla \cdot \left(b_n^2 \nabla \chi_n^{CSI}\right)}{\sum_t \left|E_{t,n}\right|^2} \tag{C.4}$$

C.2 Calculating the step update of contrast χ

While calculating the step update for the contrast of the FEM-MRCSI algorithm the relation $\chi_n^{CSI} + \beta_n d_n^{\chi}$ is incorporated into the method's cost functional

$$\begin{aligned} F\left(\chi_n^{CSI} + \beta_n d_n^{\chi}, w_{t,n}\right) &= F^{MR}\left(\chi_n^{CSI} + \beta_n d_n^{\chi}\right) F^{CSI}\left(\chi_n^{CSI} + \beta_n d_n^{\chi}, w_{t,n}\right) \\ &= \left(\left\| b_n \nabla \chi_n^{CSI} + b_n \beta_n \nabla d_n^{\chi} \right\|_D^2 + \delta_n^2 \left\| b_n \right\|_D^2\right) \\ &\quad \times \left(F^S\left(w_{t,n}\right) + F^D\left(\chi_n^{CSI} + \beta_n d_n^{\chi}, w_{t,n}\right)\right) \end{aligned} \tag{C.5}$$

$$\begin{aligned} \left\| b_n \nabla \chi_n^{CSI} + b_n \beta_n \nabla d_n^{\chi} \right\|_D^2 &= \int_D \left(b_n \nabla \chi_n^{CSI} + b_n \beta_n \nabla d_n^{\chi}\right)\overline{\left(b_n \nabla \chi_n^{CSI} + b_n \beta_n \nabla d_n^{\chi}\right)} dv \\ &= \left\| b_n \nabla \chi_n^{CSI} \right\|_D^2 + 2\beta_n \operatorname{Re}\left\langle b_n \nabla \chi_n^{CSI}, b_n \nabla d_n^{\chi} \right\rangle_D \\ &\quad + \beta_n^2 \left\| b_n \nabla d_n^{\chi} \right\|_D^2 \end{aligned} \tag{C.6}$$

$$F^D\left(\chi_n^{CSI}+\beta_n d_n^{\chi},w_{t,n}\right)=\eta_{D,n}\left\|\mathbf{E}_{t,n}\left(\chi_n^{CSI}+\beta_n d_n^{\chi}\right)-w\right\|_D^2$$
$$=\eta_{D,n}\left(\left\|\mathbf{E}_{t,n}\chi_n^{CSI}\right\|_D^2+2\beta_n\,\mathrm{Re}\left\langle\mathbf{E}_{t,n}d_n^{\chi},\mathbf{E}_{t,n}\chi_n^{CSI}-w_{t,n}\right\rangle_D\right. \quad \text{(C.7)}$$
$$\left.+\beta_n^2\left\|\mathbf{E}_{t,n}d_n^{\chi}\right\|_D^2\right)$$

By combining the equations (C.5)-(C.7) the relation that denotes the contrast step update is extracted.

$$F_n=\left[\left\|b_n\nabla\chi_n^{CSI}\right\|_D^2+\delta_n^2\left\|b_n\right\|_D^2+\beta_n^2\left\|b_n\nabla d_n^{\chi}\right\|_D^2+2\beta_n\,\mathrm{Re}\left\langle b_n\nabla\chi_n^{CSI},b_n\nabla d_n^{\chi}\right\rangle_D\right]$$
$$\times\left[2\eta_{D,n}\beta_n\,\mathrm{Re}\sum_t\left\langle\mathbf{E}_{t,n}d_n^{\chi},\mathbf{E}_{t,n}\chi_n^{CSI}-w_t\right\rangle_D+\right. \quad \text{(C.8)}$$
$$\left.F^S\left(w_{t,n}\right)+F^D\left(\chi_n^{CSI},w_{t,n}\right)+\eta_{D,n}\beta_n^2\left\|\mathbf{E}_{t,n}d_n^{\chi}\right\|_D^2\right]$$

C.3 Approximation of the divergence of the spatial contrast derivatives

In order to calculate the divergence of the spatial derivatives of the contrast, as it has already been mentioned due to the discontinuities of the base functions of the finite elements some sort of averaging must be implemented. Let's define a unitary constant vector $\hat{v}$ and a scalar function of the form $\varphi(\vec{r})$. In any region H the average value of the inner product $\hat{v}\cdot\varphi(\vec{r})$ is given by an integral with the form

$$\left\langle\hat{v}\cdot\varphi(\vec{r})\right\rangle=\frac{1}{V}\int_H\hat{v}\cdot\varphi(\vec{r})\,dv \quad \text{(C.9)}$$

where V is the area of the region H if it is two dimensional. Equation (C.9) with the help of vector calculus identities can be written as

$$\left\langle\hat{v}\cdot\varphi(\vec{r})\right\rangle=\frac{1}{V}\int_{\Gamma_H}\left\{\nabla\cdot\left[\varphi(\vec{r})\hat{v}\right]-\varphi(\vec{r})\left(\nabla\cdot\hat{v}\right)\right\}dv \quad \text{(C.10)}$$

Since the vector $\hat{v}$ is constant its divergence is equal to zero and with the help of divergence theorem the following equation is derived

$$\left\langle\hat{v}\cdot\varphi(\vec{r})\right\rangle=\frac{1}{V}\oint_{\Gamma_H}\varphi(\vec{r})\hat{v}\cdot\hat{n}dv \quad \text{(C.11)}$$

REFERENCES

[1] J. Jin, "The Finite Element Method in Electromagnetics", 2nd edition, *John-Wiley and sons INC.,* New York 2002.

[2] J.-P. Berenger, "A Perfectly Matched Layer for the Absorption of Electromagnetic Waves", *Journal of Computational Physics 114*, 1994.

[3] W. Ch. Chew, W. H. Weedon, "A 3D Perfectly Matched Medium from Modified Maxwell's with Stretched Coordinates"*, Microwave and Optical Letters,* vol. 7, no 13, September 1994.

[4] Z. S. Sacks, D. M. King, R. Lee, J.-F. Lee, "A Perfectly Matched Anisotropic Absorber for Use as an Absorbing Boundary Condition", *IEEE Transactions on Antennas and Propagation,* vol. 43, no 12, December 1995.

[5] C. Gilmore, "Towards and improved microwave tomography system", *Ph.D. dissertation*, University of Manitoba, 2010.

[6] A. Zakaria, "The Finite Element Contrast Source Inversion Method for Microwave Imaging Applications", *Ph.D. dissertation*, University of Manitoba, 2012.

[7] T. V. Yioultsis, Em. E. Kriezis, "Microwaves", *Afoi Kiriakidi,* 2008.

[8] P. M. van den Berg, R. E. Kleinman, "A Contrast Source Inversion Method", *Inverse Problems,* vol. 13, no 6, p 1607, 1997.

[9] P. M. van den Berg, A. Abubakar, "Contrast Source Inversion Method: State of the art", *Progress in Electromagnetic Research,* vol 34, pp 189-218, 2001.

[10] P. M. van den Berg, A. L. van Brockhoven, A. Abubakar, "Extended Contrast Source Inverion", *Inverse Problems,* vol 15, no 5, pp 1325, 1999.

[11] M. S. Pearce, J. A. Salotti, M. P. Little, K. McHugh, C. Lee, K. P. Kim, N. L. Howe, C. M Ronckers, P. Rajaraman, A. W Craft, L. Parker, A. Berrington de González, "Radiation exposure from CT scans in childhood and subsequent risk of leukaemia and brain tumours: a retrospective cohort study", *The Lancet,* Early Online Publication, June 2012

[12] M. Oristaglio and H. Block, "Wavefield Imaging and inversion in electromagnetics and acoustics"*, Course Notes TU Delft*

[13] J. Kaipio, E. Somersalo, "Statistical and Computational Inverse Problems", *Springer Science and Business Media*, 2004

[14] A. Abubakar, W. Hu, P. van den Berg, T. Habashy, "A Finite-Difference Contrast Source Inversion Method", *Inverse Problems,* vol 24, p. 065004 (17pp), 2008.

[15] A. Abubakar, P. M. van den Berg, "Iterative forward and inverse algorithms based on domain integral equations for three-dimensional electric and magnetic objects", *Journal of Computational Physics,* vol 195, pp. 236-262, 2004

[16] E. Chong and S. Zak, "An Introduction to Optimization", *New York: Wiley Interscience*, 2001.

[17] A. Zakaria, C. Gilmore, J LoVetri, "Finite-element contrast source inversion method for microwave imaging", *Inverse Problems,* vol 26, no 11, p. 115010, 2010

[18] I. T. Rekanos, T.V. Yioultsis, T. D. Tsiboukis, "Inverse scattering using the finite-element method and o nonlinear optimization technique", *Microwave Pulse Electromagnetics 9, ISBN 978-0-387-77844-0. Springer Science + BusinessMedia, LLC, 2010, p. 481,* vol. 1, p. 481, 2010.

[19] K. D. Paulsen, P. Meaney, M. Moskowitz, and J. S. Jr., "A dual mesh scheme for finite element based reconstruction algorithms", *IEEE Transactions on Medical Imaging*, vol. 14, no. 3, pp. 504-514, Sept 1995.

[20] A. Abubakar, P. M. van den Berg, J. J. Mallorqui, "Imaging of biomedical data using a multiplicative regularized contrast source inversion method", *IEEE Transactions on Microwave Theory and Techniques*, vol. 50, no. 7, pp. 1761-1777, July 2002.

[21] A. Abubakar, P. M. van den Berg, T. M. Habashy, H. Braunisch, "A multiplicative regularization approach for deblurring problems", *IEEE Transactionson Image Processing*, vol. 13, no. 11, pp. 1524-1532, Nov 2004.

[22] P. van den Berg, A. Abubakar, and J. Fokkema, "Multiplicative regularization for contrast profile inversion", *Radio Science*, vol. 38, pp. 23.1-23.10, 2003.

[23] A. Zakaria, J. LoVetri, "Application of multiplicative regularization to the finite-element contrast source inversion method", *IEEE Transactions on Antennas and Propagation*,, vol. 59, no. 9, pp. 3495-3498, Sept 2011.

[24] C. A. Balanis, "Advanced Engineering Electromagnetics", *John-Wiley and sons INC.,* New York 1989.

[25] P. Mojabi, J. LoVetri, "Comparison of TE and TM inversions in the framework of the Gauss-Newton method", *IEEE Transactions on Antennas and Propagation*, vol. 58, no. 4, pp. 1336-1348, 2010.

[26] B. Kooij, P. van den Berg, "Nonlinear inversion in TE scattering", *IEEE Transactions on Microwave Theory and Techniques*, vol. 46, no. 11, pp. 1704-1712, 1998.

[27] G. Otto, W. Chew, *"Inverse scattering of Hz waves using local shapefunction imaging: A T-matrix formulation",* International Journal of Imaging Systems and Technology, vol. 5, no. 1, pp. 22-27, 1994.

[28] R. F Bloemenkamp, A. Abubakar, P. M van den Berg, "Inversion of experimental multi-frequency data using the contrast source inversion method", *Inverse Problems,* vol 17, p 1611-1622, 2001.

[29] C. Yu, Lin-Ping Song, Q. H. Liu, "Inversion of multi-frequency experimental data for imaging complex objects by a DTA–CSI method", *Inverse Problems,* vol 21, pp S165–S178, 2005.

[30] Lin-Ping Song, C. Yu, "Through-Wall Imaging (TWI) by Radar: 2-D Tomographic Results and Analyses", *IEEE Transactions on Geoscience and Remote Sensing,* VOL. 43, NO. 12, December 2005

[31] R. Marklein, J. Miao, "Linear and Nonlinear Inverse Scattering Applied to Experimental Data", available online http://www.ursi.org/Proceedings/ProcGA08 papers/BP17p15.pdf

[32] A. Abubakar, T.M. Habashy, "Nonlinear inversion of multi–frequency microwave Fresnel data using the multiplicative regularized contrast source inversion," *Progress in Electromagnetics Research*, vol. 62, pp. 193–201, 2006.